UNIVERSIDADE ESTADUAL PAULISTA
"JÚLIO DE MESQUITA FILHO"
Câmpus de São José do Rio Preto

Pedro Costa Monteiro Pizzol

Impedimetric Immunosensor Based on the Sensorial Platform of Poly(o-phenylenediamine)-AuNPs and 5-metylCytosine Antibody

Presidente Prudente

2025

Pedro Costa Monteiro Pizzol

Impedimetric Immunosensor Based on the Sensorial Platform of Poly(o-phenylenediamine)-AuNPs and 5-metylCytosine Antibody

Dissertação apresentada como parte dos requisitos para obtenção do título de Mestre em Química, junto ao Programa de Pós-Graduação em Química, do Instituto de Biociências, Letras e Ciências Exatas da Universidade Estadual Paulista “Júlio de Mesquita Filho”, Câmpus de São José do Rio Preto.

Orientador: Prof. Dr. Marcos Fernando de Souza Teixeira
Coorientador: Profª. Drª. Patrícia Monteiro Seraphim

Presidente Prudente

2025

P695i

Pizzol, Pedro Costa Monteiro
Impedimetric Immunosensor Based on the Sensorial Platform of Poly(o-phenylenediamine)-AuNPs and 5-metylCytosine Antibody / Pedro Costa Monteiro Pizzol. -- São José do Rio Preto, 2025
72 p.

Dissertação (mestrado) - Universidade Estadual Paulista (UNESP), Instituto de Biociências Letras e Ciências Exatas, São José do Rio Preto
Orientador: Marcos Fernando de Souza Teixeira
Coorientador: Patrícia Monteiro Seraphim

1. Eletroquímica. 2. Química Analítica. I. Título.

Sistema de geração automática de fichas catalográficas da Unesp. Dados fornecidos pelo autor(a).

IMPACTO POTENCIAL DESTA PESQUISA

Este estudo apresenta um avanço significativo no campo dos biossensores, alinhando-se diretamente com os Objetivos de Desenvolvimento Sustentável (ODS) da Organização Mundial da Saúde (OMS), particularmente no que diz respeito ao ODS 3, que visa assegurar uma vida saudável e promover o bem-estar para todos, em todas as idades. A detecção precoce e precisa de alterações epigenéticas, como a metilação do DNA, tem o potencial de revolucionar o diagnóstico e o monitoramento de doenças complexas, como o câncer, contribuindo para a redução da mortalidade prematura por doenças não transmissíveis (meta 3.4 dos ODS). A plataforma desenvolvida, baseada em um nanocompósito de polímero π-conjugado e nanopartículas metálicas, oferece uma alternativa eficiente, sensível, seletiva, portátil e de baixo custo para a detecção de biomarcadores epigenéticos. Esse método pode ser particularmente impactante em ambientes com recursos limitados, como unidades de atenção primária à saúde, promovendo equidade no acesso a diagnósticos avançados (ODS 10 - Redução das Desigualdades).

A utilização da espectroscopia de impedância eletroquímica, combinada com a imobilização de um único anticorpo específico (anti-5-metilcitosina), simplifica o processo de análise, reduzindo custos e tempo, enquanto mantém alta sensibilidade e seletividade. Essa abordagem inovadora pode impulsionar o desenvolvimento de tecnologias sustentáveis e acessíveis, alinhando-se ao ODS 9, que prevê a construção de infraestruturas resilientes, promoção da industrialização inclusiva e sustentável, e o fomento à inovação. Além disso, o uso de oxigênio como mediador redox elimina a necessidade de reagentes adicionais, reduzindo custos e impactos ambientais, o que contribui para o ODS 12, que trata do consumo e produção responsáveis.

Ao possibilitar a detecção precoce de doenças e o monitoramento eficaz de tratamentos, essa pesquisa também apoia o ODS 17, que enfatiza parcerias e colaborações para o desenvolvimento de tecnologias inovadoras. A combinação de técnicas avançadas e materiais acessíveis posiciona o imunossensor como uma ferramenta promissora para aplicações práticas em diagnósticos clínicos e pesquisas epigenéticas, contribuindo para o avanço da saúde global e o cumprimento das metas estabelecidas pela OMS.

POTENTIAL IMPACT OF THIS RESEARCH

This study represents a significant advancement in the field of biosensors, directly aligning with the Sustainable Development Goals (SDGs) of the World Health Organization (WHO), particularly SDG 3, which aims to ensure healthy lives and promote well-being for all at all ages. The early and accurate detection of epigenetic changes, such as DNA methylation, has the potential to revolutionize the diagnosis and monitoring of complex diseases, such as cancer, contributing to the reduction of premature mortality from non-communicable diseases (target 3.4 of the SDGs). The developed platform, based on a π-conjugated polymer nanocomposite and metallic nanoparticles, offers an efficient, sensitive, selective, portable, and low-cost alternative for the detection of epigenetic biomarkers. This method can be particularly impactful in resource-limited settings, such as primary healthcare units, promoting equity in access to advanced diagnostics (SDG 10 - Reduced Inequalities).

The use of electrochemical impedance spectroscopy, combined with the immobilization of a specific antibody (anti-5-methylcytosine), simplifies the analysis process, reducing costs and time while maintaining high sensitivity and selectivity. This innovative approach can drive the development of sustainable and accessible technologies, aligning with SDG 9, which calls for building resilient infrastructure, promoting inclusive and sustainable industrialization, and fostering innovation. Furthermore, the use of oxygen as a redox mediator eliminates the need for additional reagents, reducing costs and environmental impacts, thereby contributing to SDG 12, which focuses on responsible consumption and production.

By enabling early disease detection and effective treatment monitoring, this research also supports SDG 17, which emphasizes partnerships and collaborations for the development of innovative technologies. The combination of advanced techniques and accessible materials positions the immunosensor as a promising tool for practical applications in clinical diagnostics and epigenetic research, contributing to the advancement of global health and the achievement of the goals established by the WHO.

Pedro Costa Monteiro Pizzol

Impedimetric Immunosensor Based on the Sensorial Platform of Poly(o-phenylenediamine)-AuNPs and 5-metylCytosine Antibody

Dissertação apresentada à Universidade Estadual Paulista (UNESP), Instituto de Biociências, Letras e Ciências Exatas, São José do Rio Preto, para obtenção do título de Mestre em Química.

Data da defesa: 07/03/2025

Banca Examinadora:

_____
Prof. Dr. Marcos Fernando de Souza Teixeira
UNESP – Faculdade de Ciências e Tecnologia - Campus de Presidente Prudente

_____
Prof. Dr. Silvania Lanfredi
UNESP – Faculdade de Ciências e Tecnologia – Campus de Presidente Prudente

_____
Prof. Dr. Ronaldo Spezia Nunes
UNESP – Faculdade de Engenharia e Ciências de Guaratinguetá

AGRADECIMENTOS

Gostaria de expressar meus sinceros agradecimentos:

Ao meu orientador e grande amigo, Prof. Dr. Marcos Fernando de Souza Teixeira, por acreditar em mim e por sua contribuição inestimável no desenvolvimento deste trabalho. Pelos momentos de amizade e pelas conversas enriquecedoras. Por me ajudar a me tornar uma pessoa melhor, um profissional mais capacitado e um futuro pesquisador mais preparado.

À Profa. Dra. Patrícia M. Seraphim, pela sua valiosa contribuição para este trabalho e por compartilhar seus conhecimentos, enriquecendo minha formação e pesquisa.

À Julia Furini Alquati, minha “amora” e companheira em todos os momentos. Sua presença, apoio e carinho são essenciais e representam minha maior motivação para continuar seguindo em frente. Sinto-me extremamente privilegiado e orgulhoso por ter você ao meu lado.

Aos meus pais, Ana e Renilton, e ao meu irmão, Cauê, alicerces essenciais da minha vida, expresso minha eterna gratidão por todo o amor, apoio e dedicação que sempre me ofereceram. Sei que nada disso seria possível sem o incentivo constante e a confiança que vocês depositaram em mim ao longo dessa jornada.

Ao Miquéias de Lima Portugal, por ter me acolhido com tanto carinho durante todos esses anos de graduação e mestrado, por estar ao meu lado nos momentos de dificuldade e por todas as conversas e risadas que tornaram essa jornada mais leve e especial. Sua amizade e apoio foram fundamentais para mim.

Aos colegas do laboratório GPES, Heitor, Masiero, Vinicius, Manoela, João e Arthur, pelo acolhimento, pelas conversas enriquecedoras e pelo apoio durante esses dois anos.

Aos meus grandes amigos João Pedro Gomes Balanco e Vinícius Freitas. Por estarem presentes na minha vida há mais de uma década. Apesar de seguirmos caminhos completamente diferentes, nunca perdemos o amor, a amizade e o carinho que nos unem. Obrigado por serem parte essencial da minha história.

À minha família de Campo Grande, Sorriso, Nova Esperança e Tietê, pelo imenso amor e carinho que sempre me deram. Sinto-me privilegiado por tê-los ao meu lado durante todos esses anos.

Por fim, a todos que, direta ou indiretamente, fizeram parte desta conquista, meu mais profundo agradecimento. Esta dissertação não é apenas minha, mas de todos que estiveram comigo nessa trajetória. Obrigado por fazerem parte desta história.

O presente trabalho foi realizado com apoio da Coordenação de Aperfeiçoamento de Pessoal de Nível Superior – Brasil (CAPES) – Código de Financiamento 001.

RESUMO

O avanço da pesquisa e desenvolvimento de relações entre o DNA metilado e a progressão de processos neoplásicos proporcionaram a elaboração de novas metodologias para a detecção da metilação das bases nitrogenadas e, consequentemente, o estudo do mecanismo epigenético da modulação de proteínas. O objetivo desse trabalho foi o desenvolvimento de um dispositivo baseado em um nanocompósito de nanopartículas de ouro (AuNPS) encapsulado em poli(o-fenilenodiamina) para o sensoriamento impedimétrico do nível global de DNA metilado em células. A plataforma sensorial foi construída por eletropolimerização de etapa única em uma solução contendo o monômero 1,2-fenilenodiamina e ácido cloroáurico sobre a superfície de um eletrodo circular impresso de ouro (BVT Tecnologies), demonstrando um possível encapsulamento de nanopartículas metálicas pela cadeia polimérica, apresentando uma maior área ativa e menor tempo de relaxação e maior sensibilidade frente ao O_2. A plataforma foi construída se baseando na utilização de oxigênio como mediador redox, sem a necessidade de adição de demais mediadores redox. A elaboração do imunossensor se deu pela imobilização do anticorpo 5-metilcitosina (Ab-5-mC) na superfície do dispositivo revestido com pontos de polímero-AuNPs. Cada etapa da construção do imunossensor foi analisada a partir da técnica de espectroscopia de impedância eletroquímica, permitindo avaliar os fenômenos interfaciais da plataforma, a partir de uma investigação mais detalhada das características e propriedades eletroquímicas. O mecanismo de resposta do sensor foi baseado nas alterações dos valores de impedância do sistema pela interação do analito 5-metilcitosina (5-mC) em solução tampão fosfato com o anticorpo sobre rede sensível pi-conjugada do nanocompósito. Por fim, verificou-se o desempenho analítico do imunossensor de poli(o-FD)-AuNPs que apresentou um limite de detecção para impedância imaginária e absoluta de 1,73 pg mL^{-1} e 1,18 pg mL^{-1}, respectivamente. O imunossensor apresentou um desempenho sensível e satisfatório para detecção de DNA metilado.

Palavras–chave: nanocompósito de ouro; sensor impedimétrico; DNA metilado.

ABSTRACT

Advances in research and development of relation between methylated DNA and the progression of neoplastic processes have led to the development of new methodologies for the detection of methylation of nitrogenous bases and, consequently, the study of the epigenetic mechanism of protein modulation. The objective of this work was the development of a device based on a nanocomposite of gold nanoparticles (AuNPS) encapsulated in poly(o-phenylenediamine) for impedimetric sensing of the global level of methylated DNA in cells. The sensory platform was constructed by single-step electropolymerization in a solution containing the monomer 1,2-phenylenediamine and chloroauric acid on the surface of a circular imprinted gold electrode (BVT Technologies), demonstrating a possible encapsulation of metallic nanoparticles by the polymer chain, presenting a larger active area and shorter relaxation time and greater sensitivity to O_2. The platform was built based on the use of oxygen as a redox mediator, without the need to add other redox mediators. The immunosensor was created by immobilizing the 5-methylcytosine antibody (Ab-5-mC) on the surface of the device coated with polymer-AuNPs dots. Each stage of the construction of the immunosensor was analyzed using electrochemical impedance spectroscopy technique, allowing the interfacial phenomena of the platform to be evaluated, based on a more detailed investigation of the electrochemical characteristics and properties. The sensor's response mechanism was based on changes in the system's impedance values due to the interaction of the analyte 5-methylcytosine (5-mC) in phosphate buffer solution with the antibody on the sensitive pi-conjugated network of the nanocomposite. Finally, the analytical performance of the poly(o-FD)-AuNPs immunosensor was verified, which presented a detection limit of 1.73 pg mL^{-1}.for imaginary impedance and 1.18 pg mL^{-1} for absolute impedance. The immunosensor presented a sensitive and satisfactory performance for detecting methylated DNA.

Keywords: gold nanocomposite; impedimetric sensor; methylated DNA.

LISTA DE FIGURAS

CAPÍTULO 2

CAPÍTULO 3

SUMÁRIO

Capítulo I

Introdução Geral e Objetivos da Dissertação

1.1 Introdução Geral e Objetivos da Dissertação

A análise e o prognóstico de doenças com alta morbimortalidade são fundamentais para o tratamento precoce e eficaz, impactando diretamente a qualidade de vida dos pacientes e a eficiência dos sistemas de saúde. Diante desse cenário, observa-se um crescente interesse no desenvolvimento de técnicas avançadas no campo da nanobiotecnologia, que permitem a investigação detalhada de sistemas biológicos e a criação de ferramentas diagnósticas mais precisas e acessíveis. Nesse contexto, os nanocompósitos, aliados a biomoléculas, emergem como uma abordagem promissora, pois possibilitam explorar as relações e propriedades físico-químicas de biossistemas de maneira inovadora. Esses materiais híbridos, que combinam propriedades únicas de nanomateriais com a funcionalidade de biomoléculas, têm viabilizado avanços significativos no desenvolvimento de sistemas de diagnóstico e prognóstico para diversas doenças.

Entre as metodologias eletroquímicas, destaca-se o uso de polímeros π-conjugados em conjunto com nanopartículas metálicas, que têm sido amplamente empregados como plataformas sensoriais. Essa combinação é particularmente vantajosa devido à facilidade de síntese por meio de eletropolimerização, além de proporcionar um ambiente ideal para a imobilização de uma ampla gama de entidades biológicas, como enzimas, proteínas, organelas, células, bactérias e DNA. A versatilidade desses materiais permite a criação de sensores altamente sensíveis e seletivos, capazes de detectar biomarcadores específicos com grande precisão.

Neste estudo, propõe-se o desenvolvimento de uma plataforma sensorial label-free, baseada em um nanocompósito composto por poli(o-fenilenodiamina) (poli(o-FD)) e nanopartículas de ouro (AuNPs), em conjunto com o anticorpo Ab-5-mC e o oxigênio dissolvido como sonda redox, para a detecção e quantificação global de 5-metilcitosina (5-mC). A 5-mC é um importante biomarcador epigenético, cuja detecção e quantificação são essenciais para o entendimento de processos biológicos e patológicos, como o câncer e outras doenças relacionadas a alterações epigenéticas. O imunossensor desenvolvido opera com base na resposta impedimétrica do sistema, que é influenciada pelo aumento da resistência à difusão do oxigênio devido à formação de uma barreira física após a interação antígeno-anticorpo. Essa interação ocorre diretamente na superfície do dispositivo, eliminando a necessidade de anticorpos secundários ou enzimas, o que simplifica o processo, reduz custos e aumenta a eficiência do sistema. Explorou-se o potencial de miniaturização do dispositivo, investigando-se a viabilidade de sua integração em sistemas portáteis e de baixo custo.

A viabilidade dessa abordagem é garantida pela resposta seletiva e sensível do polímero condutor à reação de redução do oxigênio dissolvido. Além disso, o método de eletropolimerização por etapa única se destaca por facilitar o encapsulamento de nanoclusters de ouro pelo polímero, contribuindo para o aumento da área ativa, estabilidade e sensibilidade da plataforma sensorial. A combinação desses elementos resulta em um dispositivo com alto desempenho analítico, capaz de operar em escalas reduzidas e com potencial para miniaturização, o que o torna adequado para aplicações portáteis e de fácil utilização.

Capítulo II

Revisão Bibliográfica

2.1. Revisão Bibliográfica

2.1.1. Cancêr e DNA Metilado

O câncer é uma das principais causas de morte em todo o mundo, representando um desafio significativo para a saúde pública. De acordo com a Organização Mundial da Saúde (OMS), em 2020, foram registrados aproximadamente 10 milhões de óbitos relacionados ao câncer, o que corresponde a quase uma em cada seis mortes globais. Além disso, estima-se que o número de novos casos diagnosticados anualmente ultrapasse 19 milhões, com projeções de aumento nas próximas décadas devido ao envelhecimento da população, mudanças nos estilos de vida e fatores ambientais. Entre os tipos mais comuns estão o câncer de pulmão, mama, colorretal e próstata, que juntos respondem por uma parcela significativa da incidência e mortalidade global (KWON; GUNASEKARAN; EOM, 2019).

A prevalência do câncer varia de acordo com a região e o nível de desenvolvimento socioeconômico. Países de baixa e média renda enfrentam desafios adicionais, como o diagnóstico tardio e o acesso limitado a tratamentos eficazes, o que contribui para taxas de mortalidade mais elevadas. No Brasil, por exemplo, o Instituto Nacional de Câncer (INCA) estimou cerca de 625 mil novos casos de câncer para o triênio 2020-2022, com destaque para os cânceres de pele não melanoma, mama e próstata. Esses dados destacam a necessidade urgente de estratégias de prevenção, diagnóstico precoce e tratamentos inovadores para reduzir o impacto dessa doença na sociedade. A busca por tecnologias avançadas, como sensores e métodos de detecção precisos, tem se tornado essencial para melhorar os resultados clínicos e a qualidade de vida dos pacientes.

Uma das características marcantes do câncer é a metilação aberrante do DNA, associada à expressão gênica anormal. A metilação do DNA é a modificação epigenética mais estudada e importante em mamíferos, regulando a expressão gênica sem alterar a sequência do DNA. O principal mecanismo envolve a metilação do carbono-5 da citosina (5-mC), mediada por enzimas chamadas DNA metiltransferases (DNMTs), que transferem grupos metil para citosinas em dinucleotídeos CpG. Esse processo é dinâmico e programado, garantindo a expressão ou silenciamento de genes específicos durante o desenvolvimento embrionário e em diferentes contextos celulares (BHOOTRA et al., 2023; CHEN et al., 2022; PAWEŁ; MAŁGORZATA, 2022).

A metilação ocorre principalmente em regiões repetitivas e corpos gênicos, enquanto as ilhas CpG (regiões ricas em CpG) geralmente permanecem não metiladas. A metilação anormal está associada a doenças metabólicas e câncer, onde se observa

hipometilação global (redução da metilação em sequências repetitivas, levando à instabilidade genômica) e hipermetilação local (silenciamento de genes supressores de tumor). Proteínas "leitoras", como as proteínas de ligação a metil-CpG (MBDs), reconhecem regiões metiladas e regulam a expressão gênica, enquanto as enzimas da família TET (Ten-Eleven Translocation) atuam como "apagadoras", convertendo 5-mC em derivados que interrompem a metilação (LI et al., 2023).

Alterações na metilação do DNA são eventos precoces no câncer, contribuindo para a instabilidade cromossômica, ativação de elementos transponíveis e silenciamento de genes supressores de tumor, destacando seu papel crítico na carcinogênese (GOUIL; KENIRY, 2019; JIN; LIU, 2018; KOCH et al., 2018; LOCKE et al., 2019; NISHIYAMA; NAKANISHI, 2021; SKVORTSOVA; STIRZAKER; TABERLAY, 2019). O equilíbrio entre metilação e desmetilação é crucial para a função gênica normal.

2.1.2. Métodos de Detecção de Mutações Genéticas

A 5-metilcitosina (5-mC) é reconhecida como um potencial biomarcador para o câncer, o que tem impulsionado o desenvolvimento de diversos métodos para sua detecção. Entre esses métodos, destacam-se o sequenciamento com bissulfito (BHATTACHARJEE et al., 2018; FAN et al., 2020; LEITÃO et al., 2018), *polymerase chain reaction* (PCR), a reação em cadeia da polimerase (PCR), técnicas óticas e eletroquímicas (OLEAN-OLIVEIRA; MONTEIRO SERAPHIM; TEIXEIRA, 2022), além do uso de equipamentos como a cromatografia líquida de alta eficiência (FRISO et al., 2002).

Essas abordagens visam possibilitar um diagnóstico precoce da doença A conversão por bissulfito é um método amplamente utilizado para distinguir entre citosinas metiladas e não metiladas, transformando citosinas não metiladas em uracila. No entanto, a conversão completa é essencial para evitar resultados falsos, e fatores como desnaturação do DNA, qualidade da amostra e condições reacionais devem ser cuidadosamente controlados. Métodos como PCR específica para metilação (MSP), sequenciamento de bissulfito, PCR digital em gotículas (ddPCR) e pirosequenciamento são descritos na literatura, cada um com suas vantagens e limitações. O MSP, por exemplo, usa primers específicos para DNA metilado e não metilado, enquanto o pirosequenciamento permite a quantificação precisa da metilação em múltiplos sítios CpG. Além disso, abordagens baseadas em enzimas de restrição sensíveis à metilação (MSRE) e enriquecimento por afinidade (como MeDIP e MAP) são apresentadas para isolar e analisar DNA metilado. Essas técnicas são úteis para estudos epigenéticos, mas exigem cuidados

com desenho de primers, qualidade do DNA e controle de reações para garantir resultados confiáveis (BHATTACHARJEE et al., 2018; FAN et al., 2020; LEITÃO et al., 2018).

Apesar da eficiência do método de bissulfito, a conversão incompleta de citosina para uracila, devido a desnaturação completa ou parcial do DNA, são problemas recorrentes (BHATTACHARJEE et al., 2018). Consequentemente, outras variações de sequenciamento de bissulfito foram implementadas ao longo dos anos para a análise de DNA metilado (HOSSAIN et al., 2017). Além das abordagens baseadas na reação com bissulfito, são propostos na literatura outros métodos analíticos convencionais, tais como a cromatografia líquida de alto desempenho (HPLC) (FRISO et al., 2002), a eletroforese capilar de alto desempenho (HPCE) (FRISO et al., 2002). Apesar de serem altamente precisas, possuem limitações devido à necessidade de alta quantidade de amostras para análise, além de serem equipamentos extremamente caros e relativamente lentos para análise (HOSSAIN et al., 2017).

O ensaio ELISA (*Enzyme-Linked Immunosorbent Assay*) é uma técnica versátil e amplamente utilizada para detectar e quantificar o DNA metilado, com diferentes variações adaptadas a necessidades específicas (**Figura 1)**. No ELISA direto, o antígeno é imobilizado na superfície da placa, seguido pela adição de um anticorpo primário conjugado a uma enzima, que, após a incorporação do substrato, gera um sinal detectável; embora seja um método simples e rápido, sua sensibilidade é limitada. A variação indireta consiste na adição de um anticorpo primário não marcado, seguido por um anticorpo secundário conjugado a uma enzima, o que confere maior sensibilidade ao ensaio devido à amplificação do sinal. A variação mais utilizada é conhecida como sanduíche, por sua vez, é especialmente indicado para a detecção de antígenos com múltiplos epítopos, utilizando dois anticorpos que "encapsulam" o antígeno, garantindo elevada especificidade e sensibilidade, sendo amplamente empregado na quantificação de biomarcadores. Por fim o ELISA competitivo é utilizado para a detecção de moléculas de pequenas dimensões ou com epítopos únicos, nas quais o antígeno presente na amostra compete com um antígeno marcado pela ligação a um anticorpo imobilizado, resultando em um sinal inversamente proporcional à concentração do antígeno (DE LA RICA; STEVENS, 2012; LOPES; SANTOS; BUENO, 2022).

Figura 1: Representação esquemática das principais variações do método ELISA.

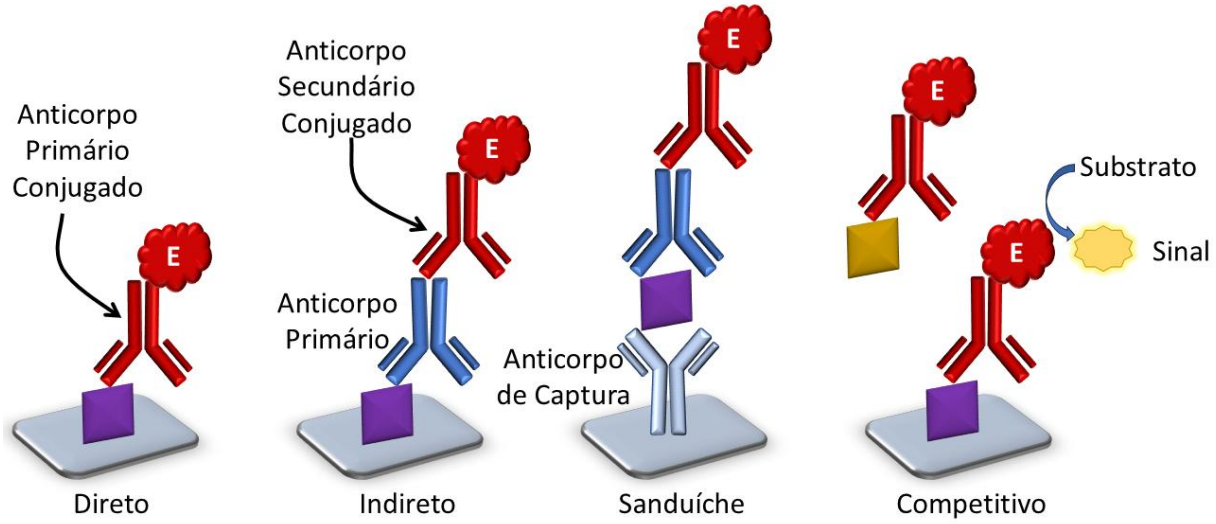

Fonte: Adaptado de (LOPES; SANTOS; BUENO, 2022).

Embora seja uma técnica sensível e amplamente utilizada, ela pode sofrer com baixa especificidade devido à possibilidade de reações cruzadas com DNA não metilado ou outras moléculas. Além disso, controles rigorosos e padronização para evitar variações nos resultados, o que pode aumentar a complexidade e o custo do processo. Outra limitação é a dependência de anticorpos de alta qualidade, aumentando o custo. Por fim, o método pode não ser ideal para amostras com baixa concentração de DNA metilado, limitando sua aplicação em certos contextos clínicos ou de pesquisa (BHOOTRA et al., 2023; PAJARES et al., 2021).

Os sensores eletroquímicos ganharam força nas últimas décadas por apresentarem ótimos limites de detecção (LOD), custo-benefício, potencial miniaturização além de não necessitarem de mão de obra especializada para realizar a quantificação. Os biossensores eletroquímicos que se baseiam em elementos de fácil reconhecimento, como anticorpos, enzimas ou sondas de oligonucleotídeos, são capazes de interagir de forma seletiva com a sequência metilada, ocorrendo a transdução para um sinal eletroquímico (BHATTACHARJEE et al., 2018). Ao longo das últimas três décadas, o desenvolvimento de imunossensores eletroquímicos apresentaram uma grande melhoria (HE et al., 2020; LEVA-BUENO; PEYMAN; MILLNER, 2020; SHARMA et al., 2019).

Os métodos eletroquímicos de análise, como voltametria, amperometria, potenciometria, impedância eletroquímica, condutometria e capacitância eletroquímica, são ferramentas essenciais para a detecção e quantificação de espécies químicas e biomarcadores. A voltametria, incluindo técnicas como voltametria cíclica (CV) e voltametria de pulso diferencial (DPV), mede a corrente elétrica em resposta a uma varredura de

potencial, sendo altamente sensível e seletiva. A amperometria, por sua vez, monitora a corrente resultante de reações de oxidação ou redução em um potencial constante, sendo amplamente utilizada em biossensores enzimáticos, como os sensores de glicose. A potenciometria mede a diferença de potencial entre eletrodos, sendo ideal para detecção de íons específicos. A espectroscopia de impedância eletroquímica, tanto faradaica quanto não faradaica, analisa a resposta do sistema a sinais de tensão alternada, permitindo a detecção de biomarcadores sem a necessidade de marcadores adicionais. A condutometria avalia a condutividade de soluções, enquanto a capacitância eletroquímica mede mudanças na capacitância da interface eletrodo-solução, sendo útil para métodos "label-free". Esses métodos destacam-se por sua sensibilidade, versatilidade e potencial de miniaturização, tornando-os fundamentais para o desenvolvimento de biossensores portáteis e aplicações de diagnóstico Point-of-Care (PoC) (LOPES; SANTOS; BUENO, 2022).

A utilização de impedância eletroquímica como técnica de transdução no desenvolvimento de sensores para mutações genéticas ganhou grande destaque, principalmente pela sensibilidade alcançada, chegando a limites de detecção na faixa de picomol por litro (A; M, 2010; E; G; A, 2015). O princípio de funcionamento dos sensores impedimétricos para mutações no DNA se assemelham aos sensores eletroquímicos descritos anteriormente, onde muitas vezes é limitado a sinais de perturbação provindos de sinalizadores redox (HE et al., 2020). Entretanto, a técnica impedimétrica demonstra ser uma grande ferramenta de transdução de sinais, devido sua alta sensibilidade a mudanças interfaciais que ocorrem no material sensível do dispositivo sensor (PEJCIC; MARCO; PARKINSON, 2006). A técnica possibilita transdução dos sensores baseados na variação de impedância total do sistema, impedância real, impedância imaginária e capacitância redox (CROUCH et al., 2001; DINCER et al., 2019; JANRAO et al., 2014; LAZANAS; PRODROMIDIS, 2022; OLEAN-OLIVEIRA et al., 2019b; PEJCIC; MARCO; PARKINSON, 2006; TREVIZAN et al., 2021).

Recentemente, no grupo de pesquisa, foi desenvolvido um sensor impedimétrico para metilação de DNA com mecanismo de detecção direta utilizando oxigênio dissolvido como uma sonda redox (OLEAN-OLIVEIRA; MONTEIRO SERAPHIM; TEIXEIRA, 2022). O imunossensor foi elaborado simplesmente pela imobilização do anticorpo 5-metilcitosina (Ab-5-mC), com alta afinidade a 5-mC, na superfície de um dispositivo revestido com pontos de azo-polímero-AuNPs. Os resultados foram promissores por possibilitar a eliminação do uso de enzima e de um segundo anticorpo na preparação do dispositivo sensorial como comumente aplicado no imunossensores.

A miniaturização de biossensores tem revolucionado o campo da análise biomolecular, oferecendo vantagens significativas, mas também apresentando desafios. Entre os pontos positivos, destacam-se a portabilidade, que permite o uso em ambientes destinados a *point-of-care*, além, de reduzir o consumo de amostras, reagentes e custos, tornando os dispositivos mais viáveis para quantificação. A miniaturização também facilita a integração com sistemas microeletrônicos, possibilitando análises rápidas e em tempo real, essenciais para diagnósticos precoces e monitoramento contínuo. No entanto, a redução de escala pode comprometer a sensibilidade e a seletividade dos biossensores, especialmente quando a concentração do analito é extremamente baixa. A fabricação de dispositivos miniaturizados também exige técnicas de nanofabricação avançadas e caras, o que pode limitar sua produção em larga escala. Além disso, a integração de múltiplas funcionalidades em um dispositivo compacto pode aumentar a complexidade do sistema, exigindo soluções inovadoras para garantir confiabilidade e reprodutibilidade (LIU et al., 2020; LOPES; SANTOS; BUENO, 2022; SOLEYMANI; LI, 2017).

Os polímeros condutores têm surgido como alternativas promissoras para a miniaturização de biossensores eletroquímicos, devido às suas propriedades únicas e versatilidade. A eletropolimerização, por exemplo, permite a deposição controlada de filmes finos e homogêneos, essenciais para a miniaturização de biossensores, representando uma alternativa viável para a miniaturização de biossensores eletroquímicos (LOPES; SANTOS; BUENO, 2022).

2.1.3. Nanocompósitos de Polímeros pi-Conjugados e Ouro

Os polímeros pi-conjugados possuem propriedades elétricas e ópticas singulares que se assemelham com os semicondutores inorgânicos. Essas propriedades existem devido às cadeias conjugadas de carbono constituídas de ligações simples (σ) e duplas (π) alternantes ao longo da cadeia macromolecular (K; ROUT, 2021; NEZAKATI et al., 2018a; YUK et al., 2020). Atualmente, os polímeros pi-conjugados são aplicados em diferentes estudos da ciência, que podem ser na proteção de corrosão em metais, baterias recarregáveis, células solares, sensores químicos e biossensores. Existem na literatura (TAJIK et al., 2020; UMOREN; SOLOMON, 2019) uma grande variedade de estruturas poliméricas, como poliacetileno, polipirrol, polifenileno, polianilina, poli(fenilenodiaminas), entre outros.

A utilização de polímeros condutores em plataformas label-free tem ganhado destaque no desenvolvimento de biossensores devido à sua versatilidade, sensibilidade e

facilidade de funcionalização, permitindo a detecção direta de alvos biológicos sem a necessidade de marcadores ou sondas adicionais. Em plataformas label-free, ou seja, não requer marcadores ou sondas adicionais, os polímeros condutores atuam como transdutores, convertendo eventos de reconhecimento molecular (como a ligação antígeno-anticorpo) em sinais elétricos mensuráveis. Essa abordagem elimina etapas complexas de rotulagem, reduz custos e simplifica o processo de detecção, tornando-a ideal para aplicações de diagnóstico rápido e Point-of-Care (NEZAKATI et al., 2018b). Assim, os polímeros condutores representam uma solução promissora para o avanço de biossensores label-free, contribuindo para o desenvolvimento de tecnologias de diagnóstico mais acessíveis e eficientes.

O oxigênio dissolvido tem sido amplamente utilizado como sonda redox em plataformas sensoriais devido à sua presença natural em sistemas biológicos e sua capacidade de participar de reações eletroquímicas. Com isso, o oxigênio dissolvido tem sido empregado em plataformas sensoriais baseadas em polímeros condutores. Nesse contexto, os polímeros condutores atuam como matrizes eficientes para a imobilização de bioreceptores (como enzimas ou anticorpos) e facilitam a transferência de elétrons durante as reações redox envolvendo o oxigênio. Essa abordagem label-free elimina a necessidade de marcadores adicionais, simplificando o design do sensor e reduzindo custos (OLEAN-OLIVEIRA et al., 2019a, 2019b, 2021, 2025; OLEAN-OLIVEIRA; MONTEIRO SERAPHIM; TEIXEIRA, 2022; OLEAN-OLIVEIRA; TEIXEIRA, 2018; TREVIZAN et al., 2021).

Nessa pesquisa, o poli(o-fenilenodiamina) foi utilizado como polímero condutor, pois apresenta uma boa estabilidade térmica, solubilidade, processabilidade e fácil obtenção (JADOUN et al., 2021; ZHANG et al., 2022). A síntese de polímeros derivados de diaminas aromáticas por meio da polimerização via oxidação do grupo amino pode resultar em duas estruturas principais: uma com anel aberto e substituição de grupo funcional (**Figura 1A**) ou outra com oxidação de ambos os grupos amino di-substituídos (**Figura 1B**). Esses processos de oxidação permitem a formação de cadeias poliméricas com diferentes arranjos estruturais, influenciando diretamente as propriedades físico-químicas e eletrônicas dos materiais obtidos. Essa versatilidade na síntese abre caminho para a criação de polímeros condutores com características ajustáveis, adequados para diversas aplicações em sensoriamento, eletrônica e armazenamento de energia.(JADOUN et al., 2021; ZHANG et al., 2022).

Figura 2: Representação da estrutura de poli(o-fenilenodiamina): **(A)** estrutura em anel aberto com grupos –NH_2 livres e –NH–. **(B)** estrutura com anel fechado (pirazina) com grupos –N= e –NH–.

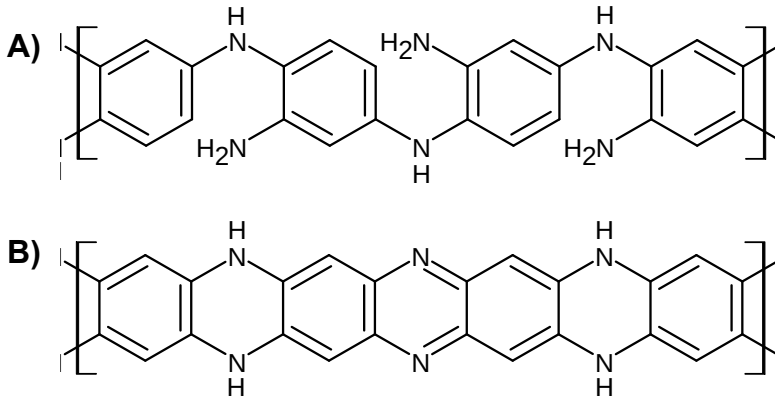

A eletropolimerização é uma técnica amplamente utilizada para a síntese de polímeros condutores, permitindo o controle preciso da espessura, morfologia e propriedades eletroquímicas dos filmes poliméricos (MARTIN; OLEAN-OLIVEIRA; TEIXEIRA, 2020; OLEAN-OLIVEIRA et al., 2019a, 2019b, 2021, 2025; OLEAN-OLIVEIRA; MONTEIRO SERAPHIM; TEIXEIRA, 2022; OLEAN-OLIVEIRA; TEIXEIRA, 2018; TREVIZAN et al., 2021). Essa abordagem oferece a vantagem de possibilitar o encapsulamento de nanopartículas metálicas durante o processo de polimerização, resultando em nanocompósitos com propriedades únicas (OLEAN-OLIVEIRA; MONTEIRO SERAPHIM; TEIXEIRA, 2022). Essa sinergia entre polímeros condutores e nanopartículas metálicas abre novas perspectivas para o desenvolvimento de materiais avançados, com aplicações em sensores, dispositivos eletrônicos e sistemas de armazenamento de energia

Dessa forma, as nanopartículas têm despertado grande interesse na área acadêmica devido à sua facilidade de síntese, ao controle das propriedades físico-químicas e à afinidade com grupos funcionais, como aminas, dissulfetos e tiols, além de possuírem propriedades eletrônicas únicas (ELAHI; KAMALI; BAGHERSAD, 2018; JAMKHANDE et al., 2019; KHAN; SAEED; KHAN, 2019; SHNOUDEH et al., 2019). No campo de sensores, as nanopartículas desempenham um papel crucial ao melhorar a estabilidade química, a condutividade elétrica e as propriedades calorimétricas dos compósitos. Além disso, elas contribuem para a amplificação do sinal, sendo amplamente utilizadas na fabricação de sensores eletroquímicos mais sensíveis, seletivos e estáveis (GUO; WANG, 2007; KIZLING et al., 2018; LU et al., 2018; XIAO et al., 2020). Essas características tornam as nanopartículas essenciais para o desenvolvimento de estratégias avançadas de detecção, ampliando as possibilidades de aplicação em diversas áreas tecnológicas

Capítulo III

Artigo Científico

3.1. Artigo Científico

Journal: ACS Applied Electronic Materials

Impedimetric Immunosensor for 5-Methylcytosine Detection Based on a Poly(o-phenylenediamine)-Encapsulated Gold Nanoparticle Platform

Pedro C. M. Pizzol[1], Miquéias L. Portugal[1], Heitor F. Trevizan[1], Patrícia Monteiro Seraphim[2], Marcos F. S. Teixeira[1*]

ABSTRACT: A novel label-free impedimetric immunosensor for the detection of 5-methylcytosine (5-mC), a key epigenetic marker, was developed based on a one-step electropolymerized nanocomposite of poly(o-phenylenediamine) (poly(o-PD)) and gold nanoparticles (AuNPs). The nanocomposite film was electropolymerized onto a screen-printed electrode (SPE) with a gold working electrode area of 0.0078 cm^2. The system was characterized by cyclic voltammetry and electrochemical impedance spectroscopy (EIS). The EIS measurements, including Nyquist, Bode, and complex capacitance plots, confirmed the successful formation of the nanocomposite and its stepwise modification with glutaraldehyde, anti-5-methylcytosine antibody (Ab-5mC), and bovine serum albumin (BSA). The immunosensor utilized the inherent redox activity of the poly(o-PD) towards dissolved oxygen as a transduction mechanism, eliminating the need for external redox mediators. The binding of 5-mC to the immobilized Ab-5mC hindered the access of dissolved oxygen to the redox-active phenazine-like units within the poly(o-PD) matrix, resulting in a measurable increase in the charge transfer resistance. The immunosensor exhibited a linear response to the logarithm of 5-mC concentration in the range of 2.5 to 160 pg mL^{-1}, with a low limit of detection (LOD) of 1.73 pg mL^{-1} and 1.18 pg mL^{-1} when using the imaginary and absolute impedance, respectively. The incorporation of AuNPs significantly enhanced the electrochemically active surface area and improved the electron transfer kinetics, contributing to the high sensitivity of the immunosensor. This work demonstrates the potential of a one-step electropolymerized poly(o-PD)-AuNP nanocomposite for the development of simple, label-free, and sensitive impedimetric immunosensors for epigenetic biomarker detection.

KEYWORDS: *Gold nanocomposite; Impedimetric Sensor; One-step Electropolymerization; Dissolved oxygen; Methylated DNA.*

1. INTRODUCTION

The convergence of materials science, nanotechnology, and electronics is driving rapid advancements in biosensing technologies, particularly for applications in early disease diagnostics. Within this interdisciplinary landscape, the development of electrochemical immunosensors for detecting epigenetic modifications, such as DNA methylation, holds significant promise.

Aberrant DNA methylation patterns, characterized by either hypermethylation or hypomethylation at the carbon-5 position of cytosine (5mC), represent a hallmark of cancer and are influenced by factors including diet, environmental exposure, and lifestyle.[1-3] These epigenetic alterations affect gene expression by modifying chromosomal proteins, thereby altering the three-dimensional conformation of the genome and influencing protein-DNA interactions.[2, 4] The clinical relevance of DNA methylation is underscored by the alarming global cancer burden, with an estimated 19.3 million new cases and 10 million deaths in 2020, as reported by the International Agency for Research on Cancer (IARC).[5] This emphasizes the urgent need for sensitive and reliable methods for early cancer detection. Bisulfite sequencing is currently the standard method and most widely used technique for 5mC detection. This method relies on the chemical conversion of unmethylated cytosine to uracil, while methylated cytosine remains unchanged. Subsequent PCR amplification and sequencing allow for the identification of methylated sites.[6, 7] Despite its widespread use, bisulfite sequencing suffers from limitations, including DNA degradation due to the harsh chemical treatment, incomplete conversion of unmethylated cytosines leading to false positives, and the requirement for specialized equipment and expertise, making it relatively time-consuming and expensive.[6-8]

Electrochemical biosensors are emerging as powerful tools for biomarker detection due to their high sensitivity, potential for miniaturization, and ability to provide rapid and quantitative results. Among various electrochemical techniques, electrochemical impedance spectroscopy (EIS) offers significant advantages for immunosensor development.[9] Unlike techniques like cyclic voltammetry, which typically focus on a single potential, or amperometry, which measures current at a fixed potential, EIS probes the system's response to a small-amplitude AC potential over a wide range of frequencies. This allows for the separation and quantification of different processes occurring at the electrode/electrolyte interface, such as charge transfer, diffusion, and double-layer charging, each characterized by a distinct time constant. This detailed information is particularly valuable for impedimetric immunosensors, where the binding of the target analyte to the immobilized antibody causes a change in the interfacial impedance. EIS is highly sensitive

to these subtle interfacial changes, enabling the detection of even very low analyte concentrations, often reaching picomolar detection limits.[10] These advantages, combined with the possibility of miniaturization using screen-printed electrodes, make EIS a highly attractive transduction method for point-of-care diagnostics. However, many traditional impedimetric immunosensors rely on the addition of exogenous redox mediators, such as hexacyanoferrate anion, to the sample solution. While these mediators can enhance the signal, their presence can also lead to complications, including increased background signal, potential interference with the biological recognition event, and the need for additional reagents.[10] In our recent work,[11] we demonstrated the use of dissolved oxygen as an intrinsic, label-free redox probe for impedimetric 5mC detection, eliminating the need for external mediators and simplifying the sensor design. This current work builds upon that foundation, exploring the use of advanced nanomaterials to further enhance sensor performance.

The choice of materials for electrode modification plays a critical role in determining the sensitivity, selectivity, and stability of electrochemical sensors, particularly in the context of miniaturization for point-of-care (POC) diagnostics. Conjugated polymers, such as poly(o-phenylenediamine) (poly(o-PD)), and metallic nanoparticles, especially gold nanoparticles (AuNPs), have garnered significant attention in the field of biosensing due to their unique electrical, optical, and catalytic properties. Poly(o-phenylenediamine), with its excellent thermal stability, solubility, processability, and ease of synthesis,[12] offers a promising matrix for stabilizing and integrating nanoparticles within electrochemical devices. Its aromatic diamine structure, capable of being oxidized to form ring structures with various functional group substitutions, provides a particularly suitable environment for the formation and stabilization of AuNPs,[11] enhancing the overall performance of the sensor. This synergy between poly(o-phenylenediamine) and AuNPs is particularly advantageous when combined with impedimetric sensing, which, due to its inherent sensitivity and potential for miniaturization, offers a promising route for developing highly specific, sensitive, and rapid POC diagnostic platforms capable of rapid and decentralized testing.[13, 14]

In this work, we demonstrate the development of an impedimetric immunosensor for DNA methylation detection that capitalizes on the synergistic properties of poly(o-phenylenediamine)-encapsulated AuNPs and the high sensitivity of EIS. The streamlined, single-step electropolymerization fabrication process, combined with the inherent advantages of these advanced materials, facilitates the development of miniaturized, efficient, and cost-effective POC diagnostic tools for early cancer detection. This approach, leveraging the robust and sensitive platform created by the synergistic combination of

poly(o-phenylenediamine) and AuNPs, pushes the boundaries of electrochemical biosensors for clinical applications, particularly in the realm of rapid, decentralized diagnostics.

2. RESULTS AND DISCUSSION

Cyclic voltammetry was used to study the formation and electrochemical properties of a nanocomposite film, prepared by the one-step electropolymerization[11, 15-17] of *o*-phenylenediamine (o-PD) and gold nanoparticles (AuNPs), resulting in AuNPs encapsulated within a poly(o-phenylenediamine) matrix (**Figure 1A**). The electropolymerization of neat poly(o-phenylenediamine) (**Figure 1B**) was also investigated for comparison.

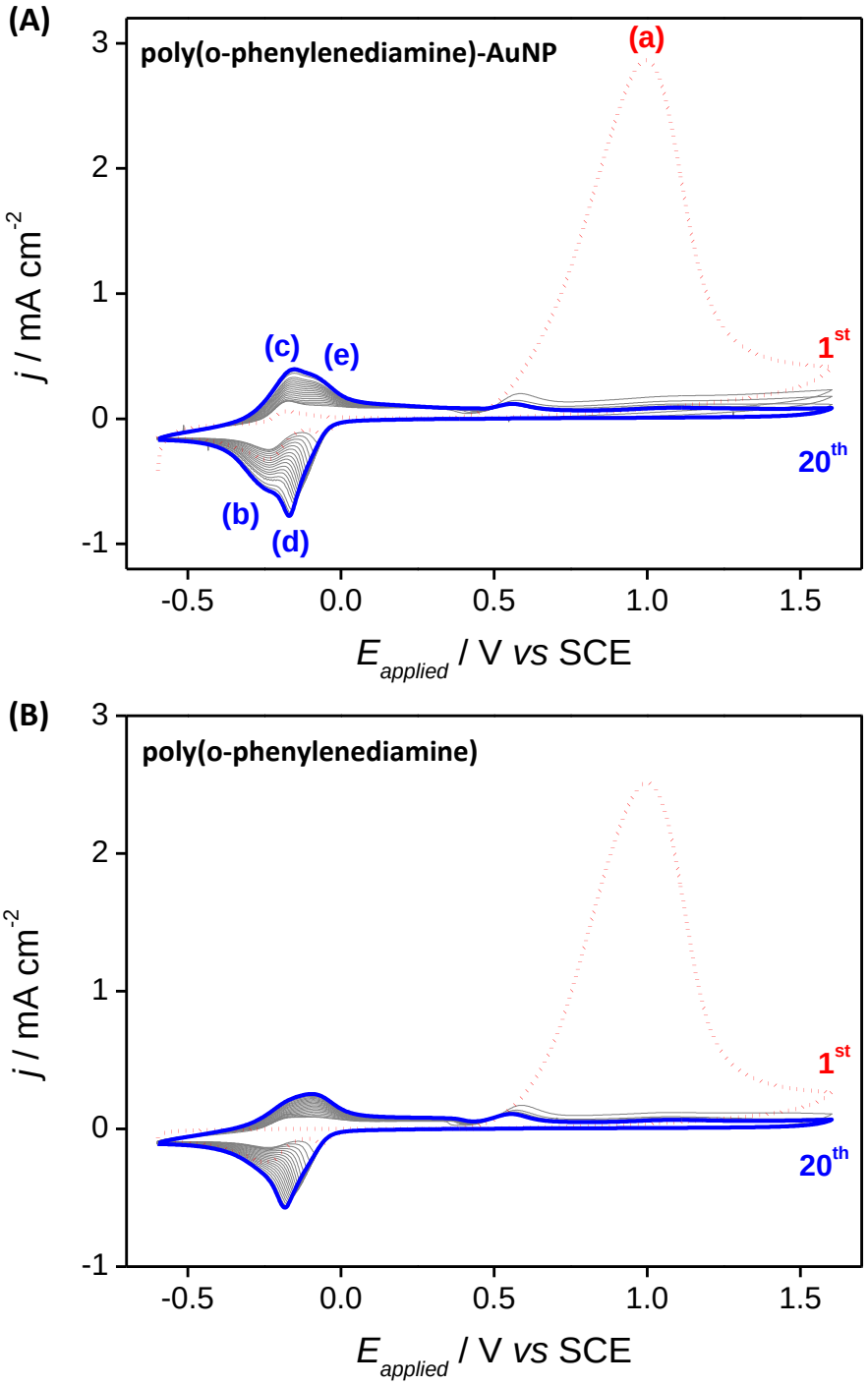

Figure 1. Cyclic voltammograms of the electrochemical processes. **(A)** One-step electropolymerization of poly(o-phenylenediamine)-AuNP nanocomposite film; **(B)** Electropolymerization of neat poly(o-phenylenediamine) film; The red dashed lines correspond to the first cycle, and the blue solid lines correspond to the 20th cycle, while the thin gray lines represent the intermediate cycles. Electrolyte: H_2SO_4 0.1 mol L^{-1}. Scan rate = 15 mV s^{-1}.

Analyzing the voltammograms for the electropolymerization of the poly(o-phenylenediamine)-AuNPs nanocomposite (**Fig. 1A**) and neat poly(o-phenylenediamine) (**Fig. 1B**), a distinct anodic peak (peak 'a' in **Fig. 1A**) is observed during the first cycle at approximately +1.0 V (vs. SCE). This peak is attributed to the oxidation of the amine groups of the o-phenylenediamine monomer, initiating the polymerization process via carbon-

nitrogen bond formation.[18] This reaction generates radical cations and, depending on the pH and applied potential, possibly radical dications. Subsequent oligomerization proceeds through a head-to-tail mechanism involving a nucleophilic attack by the amino group on the C4 position of another radical cation, leading to the formation of either open or closed chain structures (**Scheme 1A**).[19-21] Successive scans reveal two distinct redox couples (peaks 'b'/'c' and 'd'/'e') in the voltammogram of the nanocomposite. These redox processes are only faintly visible in the voltammogram of the neat polymer. The incorporation of AuNPs during the electropolymerization process appears to significantly alter the reaction pathway and the resulting polymer structure. In the case of the poly(o-phenylenediamine)-AuNPs nanocomposite, the two redox couples (**Scheme 1B**) suggest a more complex and heterogeneous structure compared to the neat polymer. This observation strongly indicates the presence of a mixture of both phenazine-like units (closed-ring) and linear chain segments (open-ring) within the nanocomposite film. The pH of the electrolyte is known to play a crucial role in determining the structure of electropolymerized poly(o-phenylenediamine).[19, 21, 22] At low pH, as employed in this study, the formation of phenazine-like units (closed-ring structures) is generally favored due to the protonation of amine groups, which influences the reactivity of the radical cation intermediates and promotes cyclization. Conversely, at higher pH values (typically above 3), a mixture of phenazine units and linear chain segments, such as N-(2-aminophenyl)aniline (open-ring), is more likely to occur. A crucial aspect of the poly(o-PD)-AuNP nanocomposite formation is the likely complexation between Au^{3+} ions (from $HAuCl_4$) and the o-phenylenediamine monomer prior to the formation of AuNPs. The observed color change upon addition of the gold salt to the monomer solution, combined with the 8:1 monomer-to-gold salt ratio, strongly suggests the formation of an Au^{3+}-monomer complex. This complexation likely plays a more dominant role than the in-situ formed AuNPs in dictating the polymer structure. The complexation can significantly alter the reactivity of the monomer.[23, 24] Au^{3+} acting as a Lewis acid, can interact with the electron-rich amino groups of the o-phenylenediamine, effectively withdrawing electron density and modifying the nucleophilicity of the monomer. To further investigate this proposed complexation, UV-Vis absorption spectroscopy was performed (see **Figure S1** in the Supplementary Material). The spectrum of the mixture of o-PD and $HAuCl_4$ in 0.1 mol L^{-1} H_2SO_4 showed a marked decrease in the absorbance at 380 nm, characteristic of tetrachloroaurate anion, and the emergence of a new, broad absorption band centered around 500 nm. These spectral changes strongly support the formation of an Au(III)-(o-PD) complex. This altered reactivity can hinder the intramolecular cyclization that leads to phenazine formation, thus favoring the formation of linear chain segments such as

diaminophenylene and N-(2-aminophenyl)aniline structures,[20] even under the acidic conditions that typically favor phenazine formation.

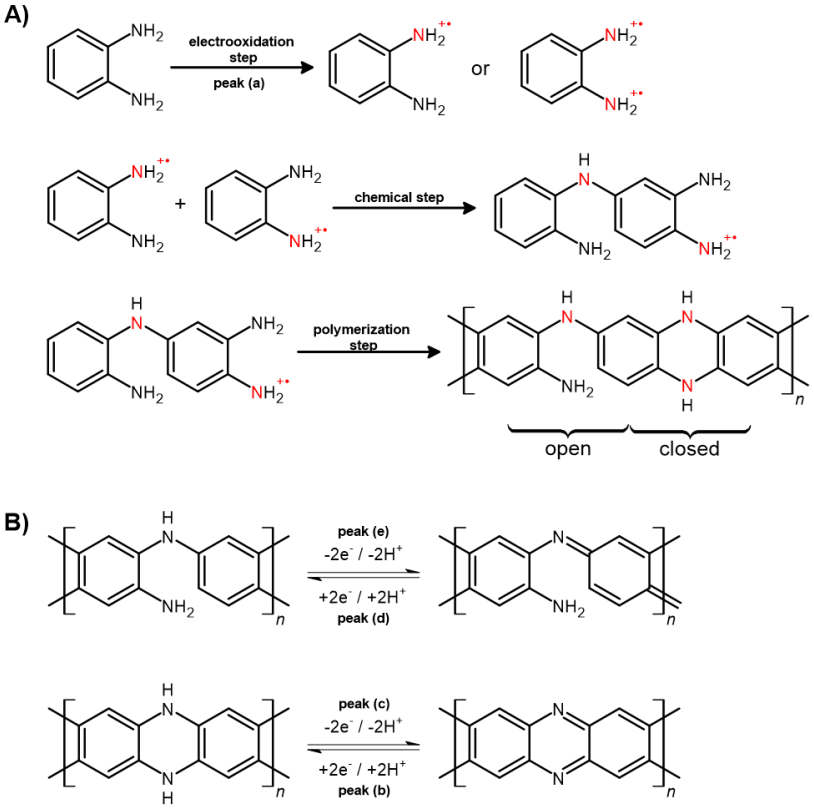

Scheme 1. Proposed mechanism for the electropolymerization of o-phenylenediamine. **(A)** Initial electrooxidation of the monomer (peak 'a') leads to a radical cation, followed by coupling with another monomer via C-N bond formation. Subsequent oxidations and coupling reactions result in the formation of open-chain (N-(2-aminophenyl)aniline units) and closed-chain (phenazine) structures. **(B)** Simplified representation of the redox processes associated with open-chain (peaks 'b'/'c') and phenazine (peaks 'd'/'e') units within the poly(o-PD) film.

Consequently, the resulting poly(o-phenylenediamine)-AuNPs nanocomposite exhibits a mixed structure comprising both closed-ring and open-ring units, as evidenced by the two distinct redox couples observed in the cyclic voltammogram (**Fig. 1A**). While the in-situ formed AuNPs contribute to the enhanced electrochemical performance of the nanocomposite, their influence on the polymer structure is likely secondary to the initial Au^{3+}-phenylenediamine complexation. This complexation event, occurring in the solution phase prior to any significant AuNP formation, appears to be the primary driver directing the polymerization pathway towards a mixed open and closed chain structure. The presence of open-chain units within this mixed structure, such as N-(2-aminophenyl)aniline segments, provides accessible primary amine groups that serve as ideal reactive sites for covalent coupling *via* glutaraldehyde. Glutaraldehyde is a crosslinking agent commonly used to immobilize antibodies onto sensor surfaces.[25, 26] This contrasts with closed-ring phenazine units, where the nitrogen atoms are incorporated into the ring structure, rendering them less accessible for conjugation. Therefore, the AuNP-induced (or, more accurately, the Au^{3+}-

complexation-induced) formation of a mixed polymer structure, with a significant proportion of open-chain units, is advantageous for the development of highly sensitive immunosensors.

The morphology of the poly(o-PD)-AuNPs nanocomposite film was characterized using SEM after the electropolymerization process (**Fig. 2A and 2B**). These images reveal the presence of structures with an irregular morphology, distributed across the substrate surface, corresponding to gold nanoclusters encapsulated within a thin layer of poly(o-phenylenediamine). **Figure 2B**, a higher-magnification SEM image, highlights these brighter features, which are attributed to the gold nanoclusters, embedded within a less electron-dense matrix consistent with the poly(o-PD). Importantly, the AuNCs are not simply dispersed on a flat surface, but appear to be coated by the polymer, with the polymer conforming to the shape of the nanoclusters. This morphology is strongly suggestive of encapsulation of the AuNCs within the poly(o-PD) matrix, a result of the one-step electropolymerization process. For comparison, a SEM image of the neat poly(o-PD) film, electropolymerized under identical conditions but in the absence of gold salt, is presented in **Figure S2** (Supplementary Material). The neat polymer film exhibits a relatively smooth and uniform morphology, distinctly different from the nanocomposite. Notably, the poly(o-PD) film lacks the brighter, irregularly shaped features attributed to the gold nanoclusters, confirming that these features in the nanocomposite (**Fig. 2B**) are indeed due to the incorporated gold. This comparison further supports the successful formation of the poly(o-PD)-AuNP nanocomposite via the single-step electropolymerization process. Further analysis of the SEM images, particularly at lower magnification (**Fig. 2A**), allowed for the construction of a particle size distribution histogram (**Fig. 2C**). The histogram reveals a broad distribution of AuNC sizes, ranging from approximately 50 to 450 nm, with an average size of around 200 nm. This wide size range, corroborated by a substantial standard deviation of approximately 93 nm, indicates that while the single-step electropolymerization method effectively produces AuNCs within the poly(o-PD) matrix, it offers limited control over the uniformity of their size and shape. This observation suggests a mechanism where the initial complexation of Au^{3+} ions by the monomer o-phenylenediamine, and possibly by the growing polymer chains, plays a crucial role. While prior studies often assume sequential reduction of Au^{3+} followed by nucleation, growth, and agglomeration of Au^{0}, our results suggest that the reduction of Au^{3+} to Au^{0} may also occur within the polymer matrix itself, with the gold ions remaining complexed to the polymer chains during the initial stages of electropolymerization. This internal reduction, possibly facilitated by the redox activity of the polymer itself, would lead to the formation of AuNCs already embedded within the poly(o-

PD) matrix. The complexation between o-phenylenediamine and Au^{3+} ions, prior to the complete reduction to Au^{0}, can significantly affect the polymerization pathway even in a low pH medium, favoring the formation of open-chain structures in detriment of the phenazine ring closure. The simultaneous nature of Au^{3+} reduction, AuNC formation, and poly(o-PD) polymerization in this single-step method presents challenges for controlling these processes independently, ultimately contributing to the observed broad size distribution and morphological heterogeneity.

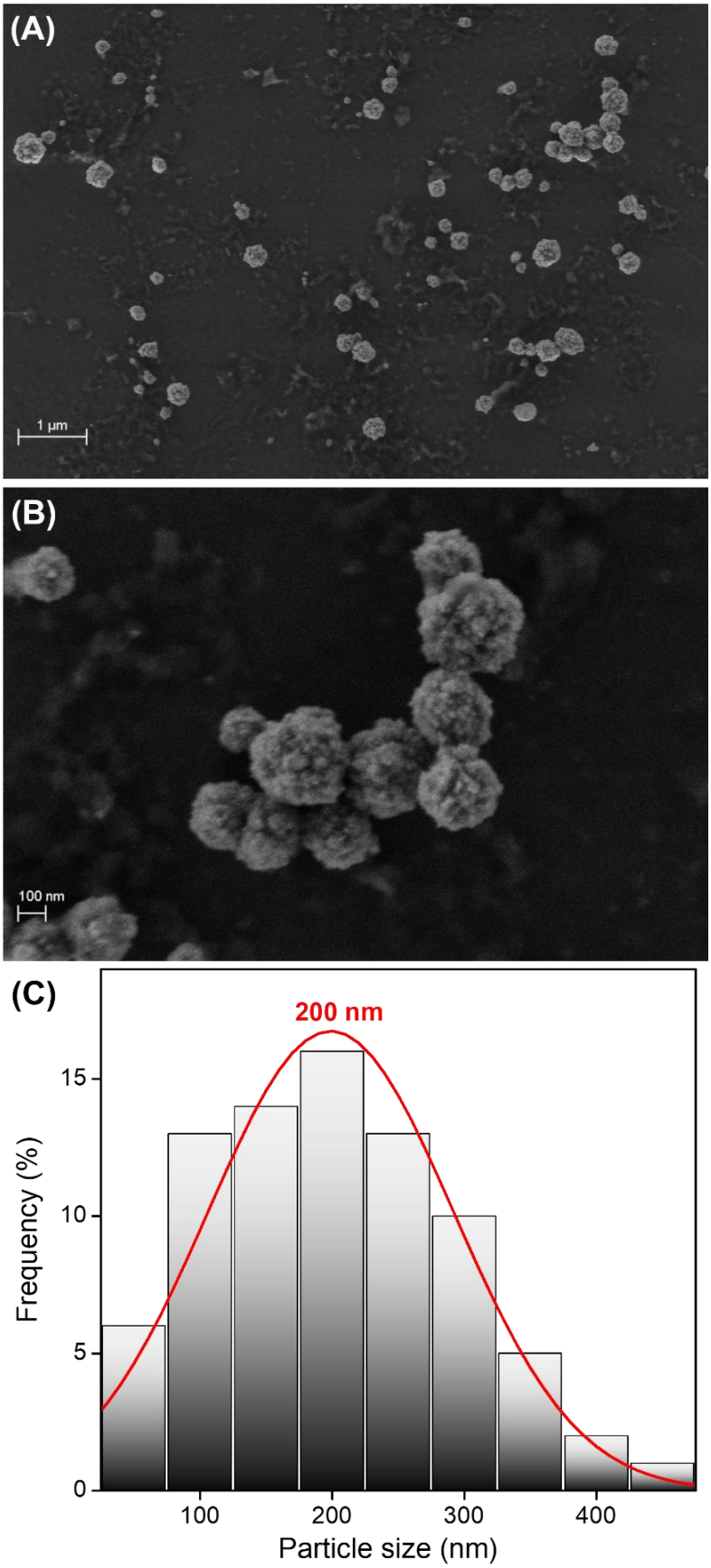

Figure 2. Morphological characterization of the poly(o-PD)-AuNP nanocomposite. **(A)** SEM image at lower magnification (Mag: 25.00 KX, HV: 3.0 kV, scale bar = 1 µm) showing the distribution of AuNCs across the substrate; **(B)** SEM image at higher magnification (Mag: 100.00 KX, HV: 5.0 kV, scale bar = 100 nm) showing the detailed morphology of encapsulated AuNCs; **(C)** Particle size distribution histogram of AuNCs, revealing an average size of around 200 nm with a standard deviation of approximately 93 nm.

2.1. Impedimetric Evaluation of the Interaction between Sensing Platform and Dissolved Oxygen

This work focuses on the development of a novel impedimetric immunosensor that utilizes the inherent redox activity of poly(o-phenylenediamine) towards dissolved oxygen as the transduction mechanism. This approach eliminates the need for exogenous redox mediators, such as hexacyanoferrate, commonly employed in traditional impedimetric sensors. By exploiting the interaction between the phenazine-like units of poly(o-PD) and dissolved oxygen, present in the sample matrix, we aim to achieve a simpler, label-free, and potentially more sensitive detection platform for methylated DNA. To evaluate the feasibility of this approach, we investigated the electrochemical behavior of both poly(o-PD) and poly(o-PD)-AuNP films using electrochemical impedance spectroscopy (EIS) in a 0.01 mol L^{-1} PBS solution saturated with O_2. **Figure 3A** presents the Nyquist plots for the poly(o-PD) and poly(o-PD)-AuNP films recorded at an applied potential of –0.4 V vs. pseudo-Ag/AgCl. This potential was chosen based on the cyclic voltammetry data (**Fig. 3E**), which indicates that significant oxygen reduction occurs in this potential range.

Both the neat polymer and the nanocomposite exhibit a similar profile in the Nyquist diagram, characterized by two overlapping, compressed capacitive arcs. While the two arcs are not clearly distinguishable by visual inspection, mathematical fitting of the impedance data using an appropriate equivalent circuit model allowed for their identification (see **Fig. 3B**). The compressed nature of the arcs and their overlap are indicative that the time constants of the processes occurring at the film/substrate and film/solution interfaces are relatively close.[27] The determined impedimetric parameters, derived from fitting the data to the proposed equivalent circuit model (**Fig. 3B**), are summarized in **Table 1**.

Table 1: Impedimetric parameters obtained from fitting the experimental data of the neat poly(o-PD) and poly(o-PD)-AuNP electrodes to the equivalent circuit model shown in **Figure 3B**. Measurements were performed in an O_2 atmosphere 0.01 mol L^{-1} PBS solution at –0.4 V vs. pseudo-Ag/AgCl. The fitting errors were below 5% for all parameters. Solution resistance (R_Ω) was found to be approximately 50 Ω cm^2 for both electrodes.

Electrode	R_{ct}	R_{film}	CPE_{dl}	CPE_{film}	α_{dl}	α_{film}
	kΩ cm^2		μF cm^{-2}			
poly(o-PD)	0.73	0.73	20.73	85.30	0.97	072
poly(o-PD)-AuNP	0.58	0.70	21.84	95.62	0.97	0.86

Significantly, the Nyquist diagram for the poly(o-PD)-AuNP nanocomposite (**Fig. 3A**) displays a smaller capacitive arc compared to that of the poly(o-PD). This difference is indicative of a lower charge transfer resistance (R_{ct}) and, consequently, enhanced electron

transfer kinetics at the nanocomposite/electrolyte interface. This improvement can be attributed to the incorporation of AuNPs, which substantially increases the electrochemically active surface area.

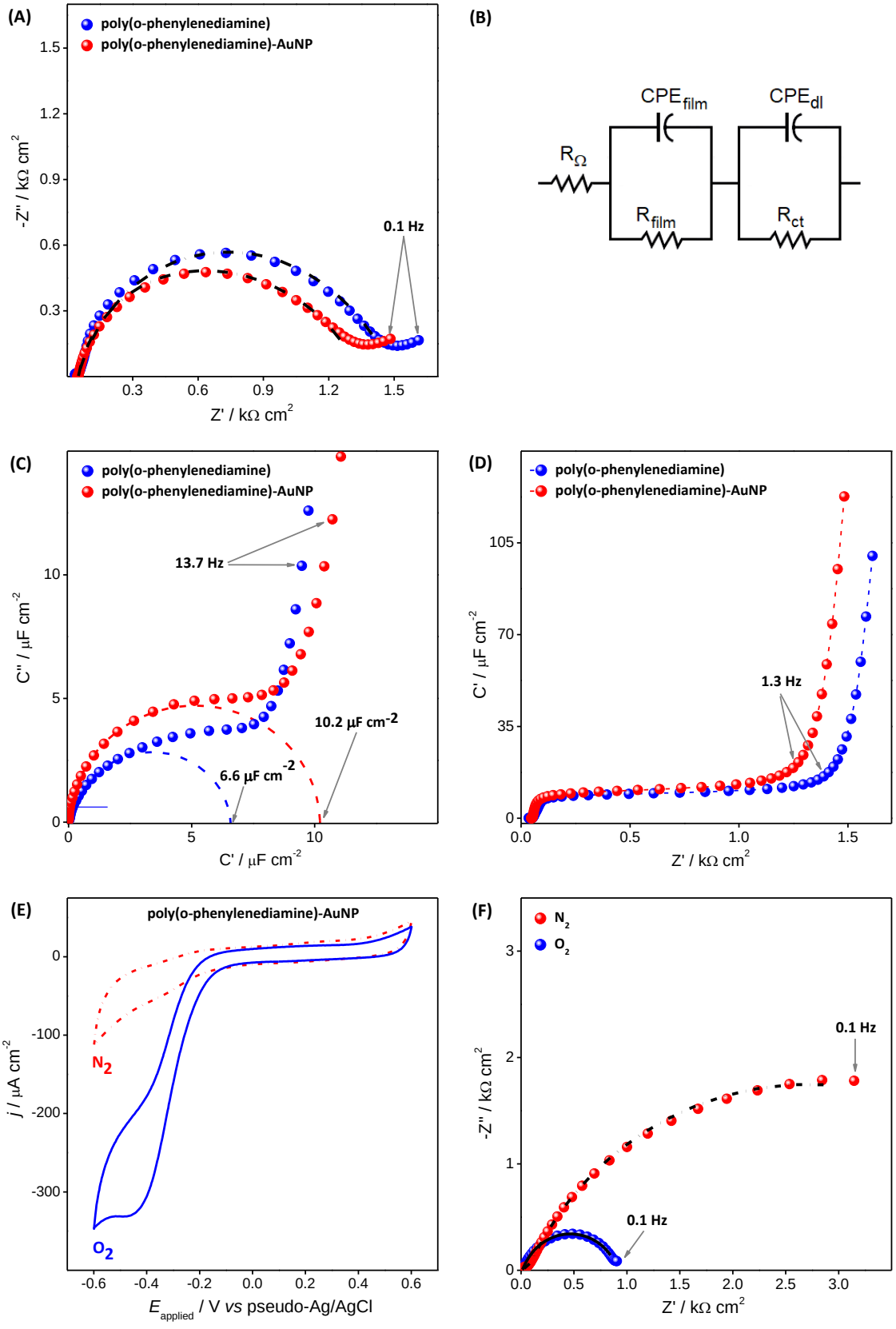

Figure 3. Electrochemical characterization of poly(o-PD) and poly(o-PD)-AuNP nanocomposite films in 0.01 mol L^{-1} PBS solution (pH 7.4). **(A)** Nyquist plots obtained at −0.4 V vs. pseudo-Ag/AgCl in O_2 solution; **(B)** Equivalent circuit model used for fitting the impedance data. R_Ω: solution resistance; R_{film} and CPE_{film}: resistance and constant phase element related to the film/substrate interface; R_{ct} and CPE_{dl}: charge transfer resistance and double-layer capacitance related to the film/solution interface and redox processes. **(C)** Complex capacitance plots in O_2 solution; **(D)** *Real capacitance* vs *Real impedance* plots in O_2 solution; **(E)** Cyclic voltammograms of the poly(o-PD)-AuNP film under N_2 and O_2 saturation at a scan rate of 25 mV s^{-1}. **(F)** Nyquist plot for the poly(o-PD)-AuNP film at an applied potential of −0.4 V (vs. pseudo-Ag/AgCl) under N_2 and O_2 saturation. Blue circles: poly(o-PD); Red circles: poly(o-PD)-AuNP nanocomposite.

The electrochemically active surface area was determined from the redox capacitance (C_{redox}) values obtained from the complex capacitance spectra (**Fig. 3C**). The C_{redox} values were extracted from the high-to-medium frequency region of the spectra, where the contribution of the redox process is dominant. The active area (Γ), expressed as the density of redox sites (mol cm^{-2}), was then calculated using the following equation:

$$\Gamma = \frac{C_{\mathrm{redox}}\, R\, T}{n^2\, F^2\, A} \quad \textbf{(1)}$$

where *R* is the ideal gas constant, *T* is the absolute temperature, *n* is the number of electrons involved in the redox reaction (assumed to be 2 for phenazine-like units), *F* is the Faraday constant and *A* is the geometric area of the electrode. This method, adapted from Bueno *et al*,[28] yielded active area values of 4.39 pmol cm^{-2} for the neat polymer and 6.78 pmol cm^{-2} for the nanocomposite. The 54% increase in active area for the poly(o-PD)-AuNP, corroborates the hypothesis that AuNPs significantly enhance the electrochemically active surface area, even when encapsulated within the polymer matrix. This is further supported by the complex capacitance data (**Fig. 3C**), which reveals a higher redox capacitance for the nanocomposite, suggesting a greater number of electrochemically active sites, specifically the redox-active phenazine-like units, available for the oxygen reduction reaction. To evaluate the electrochemical performance of the poly(o-PD) and poly(o-PD)-AuNP films towards oxygen reduction, the apparent heterogeneous electron transfer rate constant (k_0) was determined using a modified version of the Butler-Volmer equation:[29]

$$k_{app} = \frac{R\, T}{n^2\, F^2\, A\, \mathrm{R_{ct}}\, \mathrm{C_{O_2}}} \quad \textbf{(2)}$$

where R_{ct} is the redox charge-transfer resistance obtained from the Nyquist plots (**Fig. 3A**), and C_{O2} is the concentration of molecular oxygen in the bulk solution (1.38 mmol L^{-1}). The calculated k_0 values were 6.60 x 10^{-5} cm s^{-1} for the poly(o-PD) film and 8.31 x 10^{-5} cm s^{-1} for the poly(o-PD)-AuNP nanocomposite. This indicates a slightly faster electron transfer rate for the oxygen reduction reaction at the nanocomposite electrode, likely due to the increased electrochemically active surface area provided by the AuNPs.

In more detail, analysis of the real capacitance (C') vs. real impedance (Z') plot (**Fig. 3D**) elucidates the differences in oxygen response between the two materials. In the high-frequency region, both films exhibit a pronounced increase in the real component of

capacitance (C') with minimal variation in the real component of impedance (Z'). This behavior is characteristic of a capacitive response, typically attributed to the charging of the electrical double layer at the electrode/electrolyte interface.[11, 30] However, the nanocomposite displays a distinct behavior in the medium-to-low frequency range. Specifically, the nanocomposite shows a significantly lower Z' and a higher C' value compared to the neat poly(o-PD) film. This indicates a lower resistance to oxygen diffusion and a greater ability to store charge related to the oxygen redox reaction within the nanocomposite film, likely due to the increased surface area and porosity afforded by the encapsulated AuNPs. In the medium frequency range, both materials exhibit an increase in Z' and a plateau in C', characteristic of a diffusion-limited process, in this case, associated with oxygen diffusion within the film. The lower Z' plateau and higher C' plateau observed for the nanocomposite suggest enhanced oxygen diffusion and a greater density of accessible redox-active phenazine-like sites compared to the neat polymer. This enhanced response to dissolved oxygen is crucial for the sensitivity of the proposed impedimetric immunosensor.

To investigate the sensitivity of the poly(o-PD)-AuNP nanocomposite to dissolved oxygen, electrochemical impedance spectroscopy measurements were performed under both oxygen-saturated and nitrogen-saturated conditions (**Fig. 3F**). The Nyquist plots obtained at an applied potential of −0.4 V (vs. pseudo-Ag/AgCl) clearly demonstrate a significant difference in the impedance response of the nanocomposite under these two conditions. Specifically, the diameter of the capacitive arc in the medium-to-low frequency region, associated with the redox processes at the film/solution interface, is markedly smaller in the presence of oxygen compared to the nitrogen atmosphere. This observation confirms that the poly(o-PD)-AuNP nanocomposite exhibits a pronounced response to dissolved oxygen, which is attributed to the interaction between oxygen and the redox-active phenazine-like units within the poly(o-PD) matrix, as previously discussed. The smaller arc radius in the oxygen-saturated solution indicates a lower charge transfer resistance for the oxygen reduction reaction, consistent with the enhanced electron transfer kinetics facilitated by the AuNPs and the increased active surface area. These findings are crucial for the proposed application of the poly(o-PD)-AuNP nanocomposite as an impedimetric immunosensor. The sensor response will be based on changes in the impedance signal, specifically the variation in the capacitive arc, caused by changes in the local oxygen concentration at the sensor surface. Upon a poly(o-PD)-AuNP film is expected to be hindered. This restricted access will lead to an increase in the R_{ct}, resulting in a larger capacitive arc in the Nyquist plot. Therefore, the sensitivity of the immunosensor will be

directly related to the magnitude of this change in the impedance response upon exposure to the target analyte. As illustrated in **Figure 3F**, the Nyquist plots for the poly(o-PD)-AuNP nanocomposite exhibit a significant difference between oxygen-saturated and nitrogen-saturated conditions. Specifically, the diameter of the capacitive arc, associated with the film/solution interface, is markedly smaller in the presence of oxygen (R_{ct} = 0.79 kΩ cm^2) compared to that observed under a nitrogen atmosphere (R_{ct} = 2.42 kΩ cm^2). This represents a substantial decrease of approximately 26% in the charge transfer resistance, highlighting the sensitivity of the nanocomposite to dissolved oxygen. In this context, R_{ct} refers specifically to the resistance associated with the oxygen reduction reaction at the film/solution interface. Such a pronounced change in R_{ct} upon exposure to oxygen underscores the potential of the poly(o-PD)-AuNP nanocomposite for sensitive and selective impedimetric detection, based on the modulation of oxygen reduction at the electrode surface.

2.2. Immunosensor Assembly and Characterization

Figure 4A presents the Nyquist plots obtained at different stages of the immunosensor construction on the poly(o-PD)-AuNP nanocomposite platform. Each plot reflects the impedance response of the modified electrode in an oxygen-saturated PBS solution at an applied potential of −0.4 V vs. pseudo-Ag/AgCl. After the initial electropolymerization of the poly(o-PD)-AuNP nanocomposite (**Fig. 4A**, red circles), the subsequent modification with glutaraldehyde (GA) resulted in a significant increase in the diameter of the capacitive arc (**Fig. 4A**, orange circles). This is consistent with the formation of a GA layer on the electrode surface, which increases the charge transfer resistance (R_{ct}) associated with the oxygen reduction reaction. The larger arc indicates that the GA layer hinders the diffusion of dissolved oxygen to the redox-active phenazine-like units within the poly(o-PD) and/or modifies the properties of the double layer at the film/solution interface. Following GA immobilization, the next step involved the incubation with the 5-methylcytosine antibody (Ab-5mC). Intriguingly, after antibody immobilization, a slight decrease in the capacitive arc diameter was observed (**Fig. 4A**, blue circles). This corresponds to a decrease in R_{ct} compared to the GA-modified electrode. While one might expect an increase in R_{ct} due to the addition of a large biomolecule, the observed decrease suggests a more complex interplay of factors. This initial decrease in impedance is consistent with the time-dependent impedance changes observed during the optimization of the antibody incubation time (see **Figure S3B** in the Supplementary Material). One possible explanation is that the initial interaction of antibodies with the surface was not solely restricted to covalent bonding

with the GA aldehyde groups. Some antibodies might have adsorbed non-specifically or weakly onto the GA-Poly(o-PD)-AuNP surface, potentially causing conformational changes in the film, altering the local environment, or creating new pathways for electron transfer. Another factor that can induce such change is a possible residual interaction between the remaining free amine groups of poly(o-PD) and the antibody, even though such interaction is much less probable than the covalent bonding with GA. To address the potential for non-specific adsorption and to block any remaining reactive aldehyde groups of GA, a final blocking step was performed using bovine serum albumin (BSA). After the BSA incubation, the Nyquist plot (**Fig. 4A**, green circles) exhibited a significant change, with the capacitive arc returning to a size and shape similar to that observed after the GA modification step. This increase in R_{ct} after BSA addition strongly suggests that the initial decrease observed upon antibody addition was likely due to non-specific or weak interactions rather than solely to specific antibody binding to the GA linker. The BSA effectively blocked these non-specific sites and potentially displaced loosely bound antibodies, thus restoring the barrier to oxygen diffusion and leading to an R_{ct} value comparable to that of the GA-modified surface. This result highlights the importance of the BSA blocking step in minimizing non-specific binding and improving the selectivity of the immunosensor.

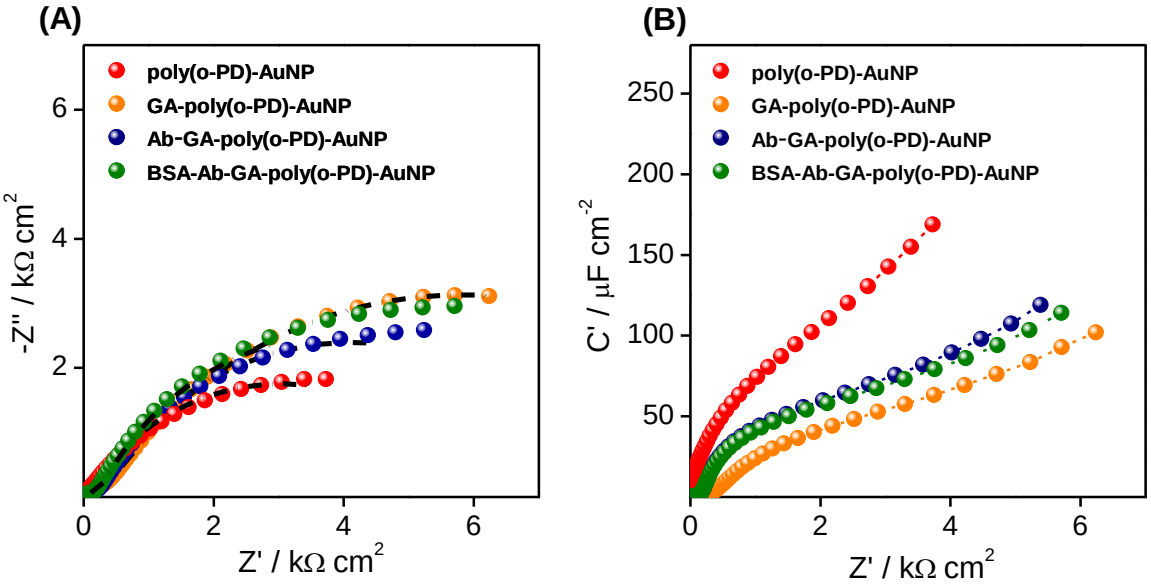

Figure 4. Stepwise electrochemical characterization of the immunosensor assembly using IS in 0.01 mol L^{-1} PBS solution saturated with O_2. **(A)** Nyquist plot and **(B)** Diagram of real capacitance as a function of real impedance, comparing the impedance response at each modification step: (i) electropolymerized poly(o-PD)-AuNP nanocomposite (red); (ii) glutaraldehyde (GA) immobilization (orange); (iii) antibody (Ab-5mC) immobilization (blue); and (iv) blocking with bovine serum albumin (BSA) (green). The Nyquist plot reveal changes in the charge transfer resistance (diameter of the semicircle), while the C' vs Z' plot highlight the changes in the real capacitance, reflecting alterations in the interfacial properties of the electrode. Measurements were performed at an applied potential of –0.4 V vs. pseudo-Ag/AgCl.

Table 2 summarizes the key impedimetric parameters obtained from fitting the experimental data to the equivalent circuit model (**Fig. 3B**) for each step of the

immunosensor assembly, as represented schematically in **Scheme 2**. The parameters, including R_{ct}, R_{film}, CPE_{dl}, and CPE_{film}, reflect the changes in the interfacial properties of the electrode upon modification with GA (Step ii), Ab-5mC (Step iii), and BSA (Step iv).

Table 2. Impedimetric parameters obtained from fitting the Nyquist plots (**Fig. 4A**) to the equivalent circuit model (**Fig. 3B**) for each step of the immunosensor assembly on the poly(o-PD)-AuNP nanocomposite. Data are presented for the following steps: (i) bare poly(o-PD)-AuNP nanocomposite; (ii) GA immobilization; (iii) Ab-5mC immobilization; and (iv) BSA blocking. All measurements were performed in an O_2-saturated PBS solution at –0.4 V vs. pseudo-Ag/AgCl.

Step	Electrode Modified	R_{ct}	R_{film}	CPE_{dl}	CPE_{film}	α_{dl}	α_{film}
		kΩ cm^2		μF cm^{-2}			
(i)	poly(o-PD)-AuNP	0.08	5.78	256	168	0.86	0.69
(ii)	GA-poly(o-PD)-AuNP	0.42	7.85	88	36	0.74	0.60
(iii)	Ab-5mC-GA-poly(o-PD)-AuNP	0.20	7.85	36	17	0.70	0.67
(iv)	BSA-Ab-5mC-GA-poly(o-PD)-AuNP	0.21	7.82	97	42	0.74	0.56

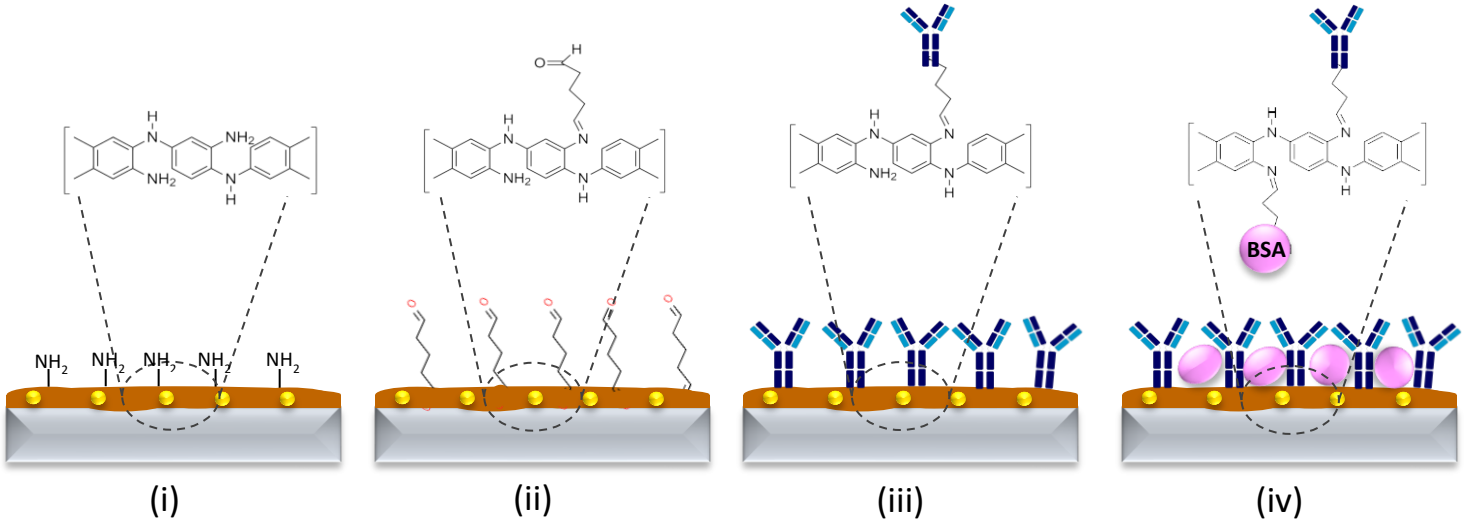

Scheme 2. Schematic illustration of the sequential steps involved in the immunosensor assembly on the poly(o-PD)-AuNP modified electrode: (i) Initial state of the electropolymerized poly(o-PD)-AuNP nanocomposite film; (ii) Covalent immobilization of glutaraldehyde (GA) via reaction with amine groups of the poly(o-PD); (iii) Antibody (Ab-5mC) immobilization through covalent bonding to the GA linker; (iv) Blocking of remaining active sites with bovine serum albumin (BSA).

Notably, the significant increase in R_{ct} after GA immobilization (Step ii) corroborates the formation of a barrier layer, as seen in the larger capacitive arc in the corresponding Nyquist plot (**Fig. 4A**, orange circles). The subsequent decrease in R_{ct} following Ab-5mC immobilization (Step iii, **Fig. 4A**, blue circles), although reversed after BSA blocking (Step iv, **Fig. 4A**, green circles), suggests an initial alteration in the film structure or interfacial properties, potentially due to non-specific adsorption. These variations in R_{ct} and specifically the changes in CPE_{dl} and CPE_{film} values, which reflect changes in the dielectric properties and the thickness of the interfacial layers, provide quantitative insights into the stepwise modification of the electrode surface. This scheme should visually represent the stepwise modification of the electrode surface, illustrating the immobilization of GA, followed by Ab-5mC, and finally the blocking with BSA on the poly(o-PD)-AuNP.

Figure 4B displays the plots of real capacitance (C') versus real impedance (Z') for the poly(o-PD)-AuNP nanocomposite at each stage of the immunosensor assembly.[11] By monitoring the changes in C' and Z', particularly in the medium-to-low frequency range, these plots provide additional insight into how the stepwise immobilization of GA, Ab-5mC, and BSA affects the diffusion of dissolved oxygen to the redox-active phenazine-like units and the resulting charge transfer processes at the electrode/electrolyte interface. After GA immobilization (orange circles), a noticeable increase in Z' is observed compared to the initial poly(o-PD)-AuNP nanocomposite (red circles). This behavior is consistent with the Nyquist plot analysis (**Fig. 4A**), confirming the formation of a GA layer that increases the resistance to charge transfer. Upon subsequent Ab-5mC immobilization (blue circles), a slight decrease in Z' is observed in the C' vs. Z' plot, mirroring the trend observed in the Nyquist plot (**Fig. 4A**). As discussed previously, this decrease in impedance, although seemingly counterintuitive, can be attributed to several factors, including non-specific or weak adsorption of the antibody, or conformational changes in the film structure that might facilitate oxygen diffusion to some extent. The final BSA blocking step (green circles) results in a significant increase in Z' across the medium-to-low frequency range, reaching values comparable to those observed after GA immobilization. This behavior corroborates the Nyquist plot analysis (**Fig. 4A**) and confirms that BSA effectively blocks the remaining active sites on the GA layer, further hindering the charge transfer process, and likely displacing any weakly or non-specifically bound antibodies. This step is crucial for minimizing non-specific interactions and improving the selectivity of the immunosensor. The C' values at the plateau in the medium frequency range follow the order: Poly(o-PD)-AuNP > Ab-5mC-GA-Poly(o-PD)-AuNP > BSA-Ab-5mC-GA-Poly(o-PD)-AuNP > GA-Poly(o-PD)-AuNP. The higher C' value for the Poly(o-PD)-AuNP nanocomposite reflects its larger electrochemically active surface area due to the incorporated AuNPs. The subsequent decrease in C' after antibody immobilization, despite the unexpected decrease in Z', might be attributed to the large size of the antibody molecule, which can reduce the overall capacitance by increasing the distance between the conductive electrode surface and the electrolyte. The further increase in C' after BSA blocking can be attributed to a combination of factors, including the non-specific adsorption of BSA, the displacement of loosely bound antibodies, and the overall modification of the interfacial dielectric properties. In conclusion, the C' vs. Z' analysis (**Fig. 4B**) complements the Nyquist plot data (**Fig. 4A**) and provides further evidence for the successful stepwise modification of the electrode surface. The observed changes in C' and Z' at each stage are consistent with the expected behavior of the system and highlight the

importance of each modification step in the development of a sensitive and selective impedimetric immunosensor based on dissolved oxygen detection.

To further investigate the impact of each modification step on the redox-active sites (phenazine-like units) of the poly(o-PD)-AuNP nanocomposite, the complex capacitance behavior was analyzed in the high-to-medium frequency region. **Figure 5** presents the complex capacitance plots (C'' vs. C') for the nanocomposite at each stage of immunosensor assembly. This analysis allows us to probe changes in the redox capacitance, which is directly related to the density of accessible phenazine-like units within the poly(o-PD) film, as previously discussed. As observed, the initial poly(o-PD)-AuNP film (red circles) exhibits a distinct capacitive arc in the medium-to-high frequency region (highlighted by the red semi-arc, for clarity), which is attributed to the C_{redox} arising from the redox-active phenazine-like units within the poly(o-PD) film.

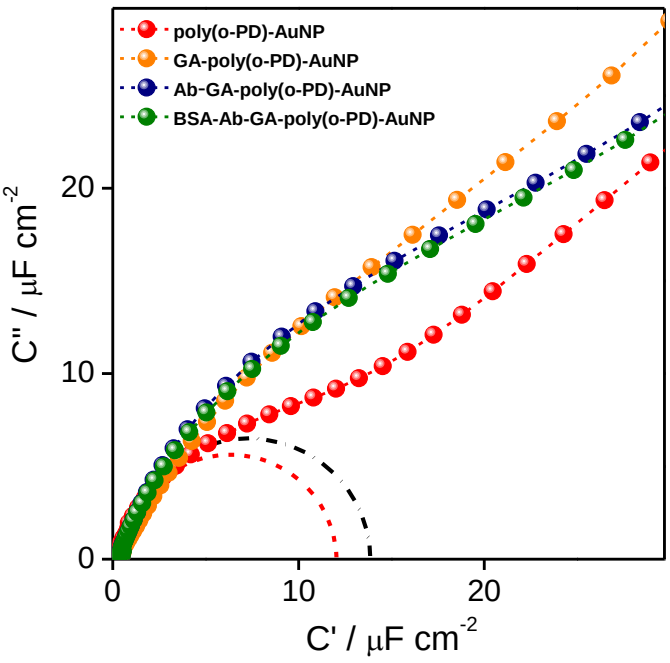

Figure 5. Complex capacitance plots (C'' vs. C') showing the evolution of the immunosensor capacitive response during each assembly step. Data for the poly(o-PD)-AuNP (red), GA-poly(o-PD)-AuNP (orange), Ab-5mC-GA-poly(o-PD)-AuNP (blue), and BSA-Ab-5mC-GA-poly(o-PD)-AuNP (green) are presented. The plots highlight changes in the redox capacitance (C_{redox}) in the medium-to-high frequency region, reflecting alterations in the accessibility and density of redox-active phenazine-like units within the poly(o-PD) film. Applied potential at –0.4 V vs. pseudo-Ag/AgCl. Frequency range: 50 kHz – 13.7 Hz.

Upon immobilization of GA (orange circles), a slight increase in the magnitude of the capacitive arc is observed in the medium-to-high frequency region. The observed increase can be attributed to two primary effects. Firstly, the binding of GA to the primary amine groups of the poly(o-PD) may induce conformational changes in the polymer chains. These conformational changes could potentially alter the packing density and arrangement

of the polymer chains, leading to a slight increase in the measured redox capacitance.[31] Secondly, although GA is not typically considered a redox-active molecule, its presence at the electrode interface and the cross-linking reactions it undergoes might create a local chemical environment that slightly modifies the electronic structure of the phenazine-like units. For example, the formation of imine bonds between GA and the polymer could influence the electron density and, consequently, the redox potential of the phenazine-like units, leading to a slightly higher apparent redox capacitance. While further investigation is needed to fully elucidate the exact mechanism, these conformational changes and localized chemical effects offer plausible explanations for the observed subtle increase in C_{redox} after GA immobilization. Following antibody immobilization (blue circles) and BSA blocking (green circles), the magnitude of the capacitive arc remains relatively unchanged compared to the GA-modified electrode. This observation suggests that while these steps are crucial for the immunosensor's functionality, they do not significantly alter the number of redox-active phenazine-like units that were made available after the GA modification. The stable C_{redox} values at these stages indicate that the oxygen reduction process, which is central to the sensor's operating principle, is maintained throughout the immunosensor assembly. This also confirm the successful immobilization of both the antibody and BSA, showing that there was no significant desorption of the previous layer.

2.3. Impedimetric Detection of 5-methylcytosine using the Immunosensor

To evaluate the performance of the developed immunosensor, its response to different concentrations of 5-methylcytosine (5-mC) was assessed using standard solutions ranging from 1.25 pg mL^{-1} to 160 pg mL^{-1} in phosphate buffer solution. 5-mC, the primary epigenetic marker of DNA methylation in eukaryotes, was chosen as the target analyte due to its critical role in gene regulation and its involvement in various biological processes, including the development of cancer. Furthermore, the use of 5-mC as a standard aligns with established protocols for DNA methylation analysis and allows for a reliable evaluation of the sensor performance.

As shown in the Nyquist plot (**Fig. 6A**), increasing the 5-mC concentration in the solution led to a corresponding increase in the diameter of the capacitive arc. This is attributed to the specific binding of 5-mC to the immobilized antibodies (Ab-5mC), creating a physical barrier on the electrode surface that hinders the diffusion of oxygen to the redox-active sites and consequently increases the charge transfer resistance (R_{ct}). The analytical curve was constructed by plotting the imaginary impedance values (-Z''), corresponding to the last point of each spectrum, against the 5-mC concentration. The -Z'' vs. 5-mC

concentration plot exhibited a Michaelis-Menten-like behavior, characteristic of the saturation profile of the antibody binding sites. To achieve a linear relationship, a logarithmic transformation was applied to the 5-mC concentration, as shown in **Figure 6B**. The resulting plot (**Fig. 6B**) exhibited linearity over the concentration range of 10.0 to 160 pg mL^{-1}, as described by **Eq. 3**.

$$Z''(k\Omega\ cm^2) = 0.160\ (\pm 0.015) + 0.157\ (\pm 0.011)\ \log([5mC](pg\ mL^{-1}) \quad (r = 0.9929) \textbf{ (3)}$$

Another way to analyze the sensor performance was to monitor the absolute impedance (|Z|), which is the magnitude of the complex impedance vector (calculated as the square root of the sum of the squares of the real and imaginary impedance components). **Figure 6C** shows the influence of the 5-mC concentration on the absolute impedance as a function of frequency. At low frequencies (100 Hz to 0.1 Hz), a clear increase in |Z| is observed with increasing 5-mC concentration. This behavior confirms that the binding of 5-mC to the immobilized antibodies hinders the electron transfer process, leading to an increase in the overall impedance. To further quantify this relationship, the absolute impedance values at a fixed frequency of 0.10 Hz were extracted from the Bode plots (**Fig. 6C**) and plotted against the logarithm of the 5-mC concentration (**Fig. 6D**). This plot, analogous to the calibration curve derived from the imaginary impedance data (**Fig. 6B**), exhibits a linear response within the concentration range of 2.50 to 160 pg mL^{-1}. The linear equation for this relationship is presented in **Eq. 4**, with a corresponding R-squared value of 0.9990, indicating a good linear fit. The linear relationship between |Z| and the logarithm of the 5-mC concentration further validates the immunosensor ability to quantitatively detect 5-mC within the tested range.

$$|Z|(k\Omega\ cm^2) = 1.13\ (\pm 0.01) + 0.28\ (\pm 0.01)\ \log([5mC](pg\ mL^{-1}) \quad (r = 0.9990) \textbf{ (4)}$$

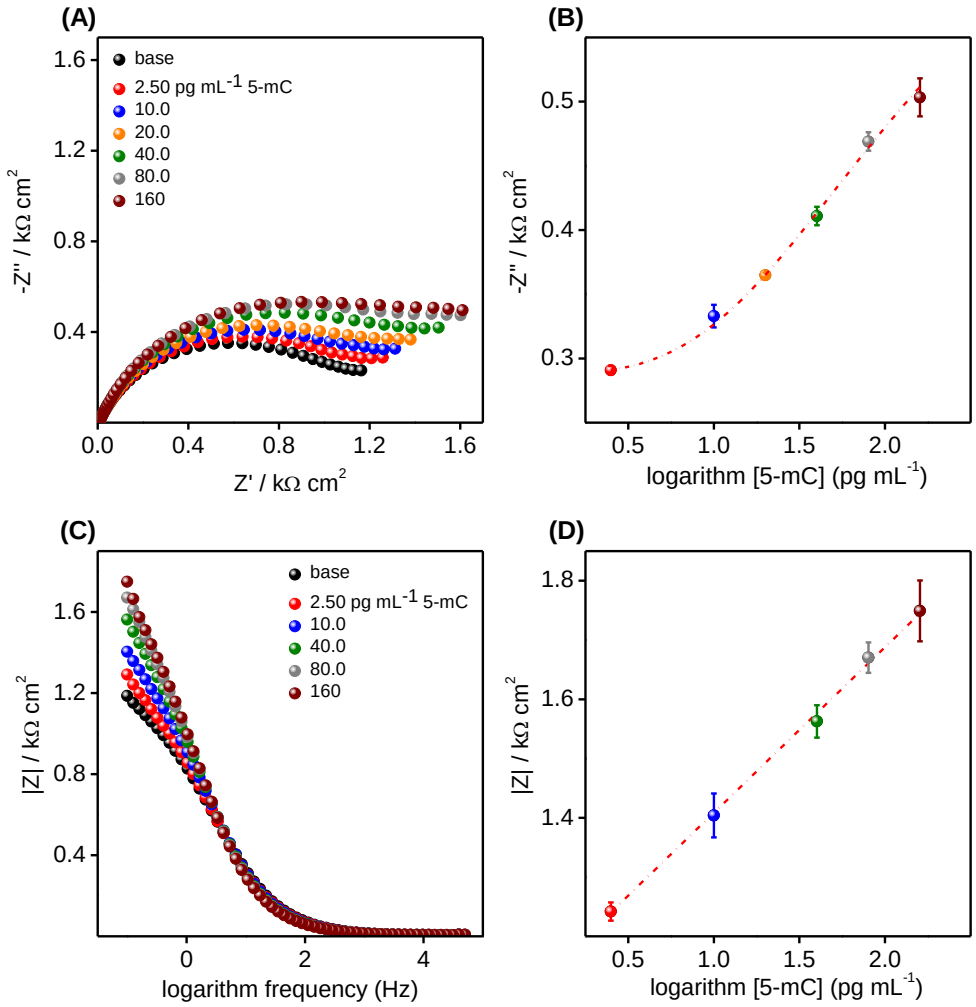

Figure 6. Electrochemical evaluation of the immunosensor response to 5-methylcytosine (5-mC). **(A)** Nyquist plots for increasing concentrations of 5-mC. **(B)** Calibration curve derived from the imaginary impedance (Z'') values at 0.10 Hz plotted against the logarithm of 5-mC concentration. **(C)** Bode plots of absolute impedance (|Z|) as a function of the logarithm of frequency for different 5-mC concentrations. (D) Calibration curve derived from the absolute impedance (|Z|) values at 0.10 Hz plotted against the logarithm of 5-mC concentration. All measurements were performed in 0.01 mol L^{-1} PBS (pH 7.4) under O_2. Error bars represent the standard deviation (n=3).

The limits of detection (LODs) were determined by fitting the non-linear response of the immunosensor to a four-parameter logistic (4PL) equation, a model commonly employed to describe sigmoidal curves in immunoassays.[32, 33] The 4PL equation was employed in this work due to its versatility and applicability to various immunoassay formats, as it can effectively capture the non-linear relationship between analyte concentration and the measured signal. The 4PL equation can be described as:

$$y = A_2 + [(A_1 - A_2)/(1 + (x/x_0)^p)] \quad \textbf{(5)}$$

where y is the measured response (impedance signal), x is the analyte concentration (5-mC), A_1 and A_2 are the minimum and maximum asymptotes of the curve, respectively, p is the Hill slope (which reflects the steepness of the curve), and x_0 is the inflection point (also known as the EC50). The parameters were estimated using non-linear

regression analysis performed with OriginPro software. The LOD was then calculated as the analyte concentration corresponding to a signal three standard deviations above the mean blank signal. This approach, using the fitted 4PL equation, provides a more accurate estimation of the LOD compared to methods relying on linearized data, as it accounts for the inherent non-linear nature of the immunosensor response. The 4PL parameters obtained from the fitting procedure, along with the mean blank signal and the calculated LOD, are presented in **Table 3**.

Table 3. Summary of the LODs obtained from the analysis of imaginary impedance (Z'') and absolute impedance (|Z|) data, along with the 4PL fitting parameters.

Parameter	Z'' Data	|Z| Data
Lower Asymptote (A_1) kΩ cm^2	0.277 (± 0.003)	1.18 (± 0.01)
Upper Asymptote (A_2) kΩ cm^2	0.572 (± 0.022)	1.84 (± 0.10)
Inflection Point (x_0) pg mL^{-1}	46.1 (± 8.61)	27.1 (± 1.09)
Hill Slope (p)	1.03 (± 0.10)	0.943 (± 0.146)
r^2	0.9980	0.9941
LOD pg mL^{-1}	1.73	1.18

The limits of detection (LODs) for 5-mC were determined to be 1.73 pg mL^{-1} and 1.18 pg mL^{-1} based on the analysis of the imaginary impedance (Z'') and absolute impedance (|Z|) data, respectively. These values compare favorably with those reported for other 5-mC sensors,[11, 34, 35] which typically range from 0.64 to 13760 pg mL^{-1}, indicating the good sensitivity of the developed immunosensor. The slightly lower LOD obtained from the |Z| data may be attributed to the fact that the absolute impedance incorporates information from both the real (resistive) and imaginary (capacitive) components of the impedance, potentially capturing subtle changes in both resistive and capacitive properties of the interface at very low 5-mC concentrations. In contrast, the imaginary impedance (Z'') primarily reflects changes in the capacitive behavior. While both parameters provide valuable and complementary information about the sensor response, the choice of which to use for quantification may depend on the specific application and the desired emphasis. The ability to analyze both Z'' and |Z| provides flexibility in data interpretation and potentially allows for a more comprehensive understanding of the interfacial processes occurring upon 5-mC binding. Importantly, these LODs are well below the clinically relevant concentration range for 5-mC in biological samples,[36, 37] demonstrating the potential of this immunosensor for practical applications. To further contextualize the performance of our immunosensor, a detailed comparison with previously reported electrochemical 5-mC sensors[34, 35, 38-41] is provided in **Table S1** (Supplementary Material).

2.4. Selectivity Studies

To evaluate the selectivity of the developed poly(o-PD)-AuNP immunosensor in the context of DNA methylation analysis, its response to 5-mC was assessed in the presence of equimolar concentrations (20 pg mL^{-1}) of cytosine, guanine, adenine, and uracil. These nucleobases, inherent components of DNA and structurally similar to 5-mC, represent potential interferents. Figure 7 presents the results of these selectivity studies, with relative responses calculated using both imaginary impedance (Z'', Fig. 7A) and absolute impedance (|Z|, Fig. 7B) values at 0.10 Hz. In both cases, the response to 5-mC alone was used as the reference (0% relative response). The error bars represent the standard deviation of triplicate measurements (n=3). As can be seen from Figure 7, the presence of the interfering bases resulted in only minor changes in both the Z'' and |Z| signals compared to the response of 5-mC alone. The relative responses for all interferents were below ±5%. Notably, cytosine and uracil caused a slight decrease in the impedance signal (negative relative response), while guanine and adenine led to a small increase. These small variations are within the range of experimental error, and indicate that the immunosensor exhibits good selectivity for 5-mC over the tested interferents. One possible explanation for the slight decrease in impedance observed with cytosine and uracil is a weak, non-specific binding of these nucleobases, both pyrimidines like 5-mC itself, to the anti-5-mC antibody. Although with significantly lower affinity than 5-mC, this interaction may displace a small amount of pre-bound 5-mC. Consequently, the slight displacement of 5-mC by these molecules could lead to a slightly increased oxygen access to the redox-active phenazine-like units of the poly(o-PD) film, resulting in a lower charge transfer resistance and, consequently, a decreased impedance signal. Although this interaction is much weaker than the specific 5-mC/antibody interaction, it may contribute slightly to the observed behavior. It is important to emphasize that, even with these minor negative responses, the overall selectivity of the immunosensor for 5-mC remains high, since the impedance changes induced by the interferents are substantially smaller than the response to 5-mC itself. In summary, this high selectivity can be mainly attributed to the specificity of the antigen-antibody interaction between 5-mC and the immobilized Ab-5mC. The results demonstrate that the immunosensor is able to selectively detect 5-mC even in the presence of structurally similar molecules.

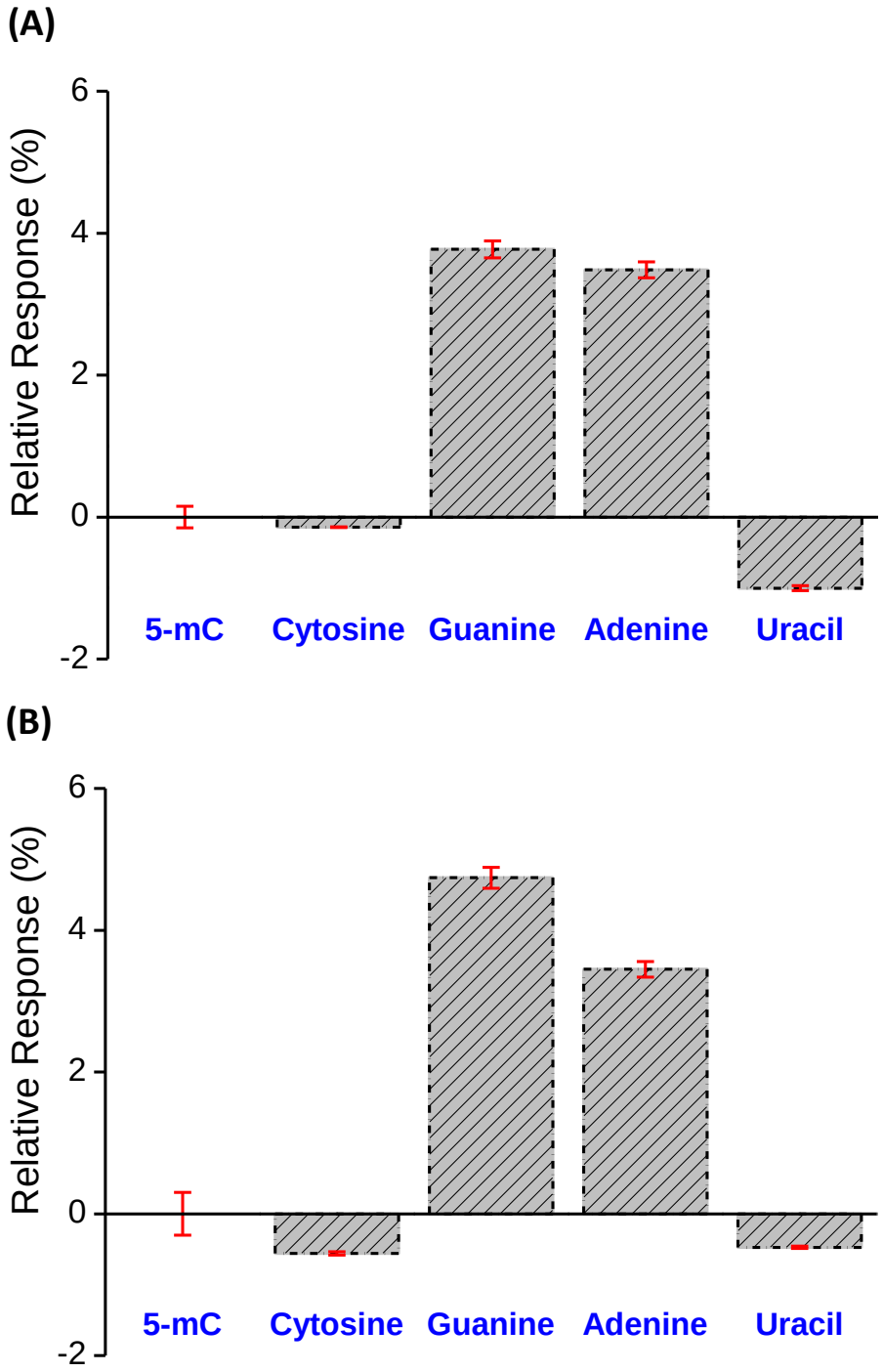

Figure 7. Selectivity of the poly(o-PD)-AuNP immunosensor. **(A)** Relative response (%) of the immunosensor to 5-mC (20 pg mL^{-1} alone and in the presence of equimolar concentrations of cytosine, guanine, adenine, and uracil, calculated from the imaginary impedance (Z'') at 0.10 Hz. **(B)** Relative response (%) calculated from the absolute impedance (|Z|) at 0.10 Hz. The response to 5mC alone is used as the reference (0%). Error bars represent the standard deviation of triplicate measurements (n = 3).

3. CONCLUSION

A label-free impedimetric immunosensor for 5-methylcytosine (5-mC) detection was successfully developed using a one-step electropolymerized poly(o-phenylenediamine)-gold nanoparticle nanocomposite. The optimized immunosensor exhibited a low limit of detection (1.73 pg mL^{-1} for imaginary impedance and 1.18 pg mL^{-1} for absolute impedance) and good sensitivity. The inter-electrode reproducibility was evaluated, with a relative standard deviation (RSD) of 0.69% for the imaginary impedance at 0.10 Hz (Supplementary Material, **Fig. S4**). The enhanced performance is attributed to the increased electrochemically active surface area provided by AuNPs and their influence on poly(o-PD) film formation, favoring a mixed structure with accessible redox-active phenazine-like units. Importantly, this platform utilizes dissolved oxygen as the redox probe, simplifying the system. Using dissolved oxygen as the redox probe simplifies the system. The impedance changes upon antibody-antigen binding demonstrate the potential of this nanocomposite for sensitive detection of DNA methylation. The developed platform holds promise for a simple and cost-effective tool for 5-mC detection in clinical diagnostics. While this work has demonstrated the promising performance of the poly(o-PD)-AuNP immunosensor in standard solutions, future studies will focus on validating its performance in complex biological matrices, such as serum or saliva. These matrices contain a variety of potentially interfering substances that could affect the sensor response. Strategies to mitigate matrix effects, such as sample pre-treatment, optimization of the BSA blocking step, and the use of highly selective antibodies, will be explored to ensure the reliable and accurate detection of 5mC in real-world samples.

4. EXPERIMENTAL SECTION

All electrochemical measurements were performed using a PalmSens4 potentiostat controlled by the PSTrace 5.10 software. The sensor platform was a screen-printed electrode (SPE) from BVT Technologies (model BVT-AC1.WS.R1.DW1), comprising a three-electrode configuration: a mixed Ag/AgCl (65%/35%) pseudo-reference electrode (RE), a platinum alloy counter electrode (CE), and a gold working electrode (WE) with a geometric area of 0.0078 cm^2.

The electropolymerization parameters for film formation, including scan rate, potential window, number of cycles, monomer concentration, and gold salt concentration, were based on previous studies conducted by the research group.[11] The nanocomposite (poly(o-PD)-AuNP) and the neat polymer (poly(o-PD)) films were synthesized via a single-

step cyclic voltammetry technique.[11, 15-17] The potential was cycled between −0.7 V and +1.6 V vs. pseudo-Ag/AgCl for 20 cycles at a scan rate of 15 mV s^{-1}. The electropolymerization was carried out in a nitrogen-saturated aqueous solution containing 0.80 mmol L^{-1} *o*-phenylenediamine (Sigma-Aldrich), 0.10 mmol L^{-1} $HAuCl_4$ (Sigma-Aldrich) for the nanocomposite, and only 0.80 mmol L^{-1} of o-phenylenediamine for the neat polymer. Both solutions contained 0.10 mol L^{-1} H_2SO_4 as the supporting electrolyte. After electropolymerization, the modified SPEs were rinsed with distilled water and stored in a plastic container until further use.

Immunosensor assembly was performed in three distinct steps. First, 2.0 µL of a 1% (m/v) glutaraldehyde (GA) solution (Sigma-Aldrich) was drop-casted onto the surface of the nanocomposite-modified WE. The electrode was then rinsed with 0.01 mol L^{-1} phosphate-buffered saline (PBS) solution (pH 7.40) to remove the excess GA. Next, 2.0 µL of a 1.0 µg mL^{-1} solution of 5-methylcytosine monoclonal antibody (Ab-5mC, GT4111 – Thermo Fisher) was pipetted onto the GA-modified surface, allowing for covalent immobilization via imine bond formation. The optimal reaction time for both GA with the poly(o-PD)-AuNP nanocomposite, and for the Ab-5mC immobilization, were determined by monitoring the changes in the Nyquist plots over time using electrochemical impedance spectroscopy (EIS). The optimized reaction times that resulted in stable impedance responses, indicating saturation of the available binding sites, were 5 minutes for GA and 10 minutes for Ab-5mC, respectively (see **Figure S3** in the Supplementary Material).

Electrochemical impedance spectroscopy (EIS) measurements were carried out in 0.01 mol L^{-1} PBS (pH 7.40) under an O_2 saturated atmosphere. A sinusoidal potential perturbation with an amplitude of 10 mV was applied at a DC potential of −0.40 V vs. pseudo-Ag/AgCl. The frequency was scanned from 50 kHz to 0.10 Hz. All impedance spectra were modeled using the EIS Spectrum Analyzer software, and a constant phase element (CPE) was used instead of an ideal capacitor to account for the non-ideal behavior of the system. The errors presented for the mathematical adjustments were less than 5%. The CPE impedance is defined by **Eq. 6**:

$$z_{CPE} = \frac{1}{Q(j\omega)^{\alpha}} \quad \textbf{(6)}$$

where Q (S s^{α}) is a frequency-dependent parameter, *j* is the imaginary unit ($\sqrt{-1}$), ω is the angular frequency ($\omega = 2\pi f$, where f is the frequency in Hz), and α is the CPE exponent (a dimensionless value between 0 and 1). The exponent α represents the phase angle of the CPE and reflects the non-ideality of the capacitive behavior. When α = 1, the

CPE behaves as an ideal capacitor; when α = 0, it behaves as an ideal resistor. The real (C') and imaginary (C'') components of the capacitance were calculated using **Eqs 7** and **8**:

$$C' = \frac{-Z''}{\omega|Z|^2} \quad \textbf{(7)}$$

$$C'' = \frac{Z'}{\omega|Z|^2} \quad \textbf{(8)}$$

where $|Z|$ represents the absolute impedance, which can be calculated using **Eq. 9**:

$$|Z| = \sqrt{\left[Z'^2 + Z''^2\right]} \quad \textbf{(9)}$$

The concentration of dissolved oxygen in the 0.01 mol L^{-1} PBS solution (pH 7.40) was determined using a calibrated, commercially available dissolved oxygen meter (Hanna, HI9146-04). The solution was saturated with O_2 gas prior to the measurements, and the concentration was measured at room temperature (25 °C) to be 1.38 mmol L^{-1}.

To evaluate the selectivity of the fabricated immunosensor, its response to 5-mC was investigated in the presence of potential interferents. The following nucleobases were selected as interferents: cytosine, guanine, adenine, and uracil (all from Sigma-Aldrich). For the interference studies, solutions containing a fixed concentration of 5-mC (20 pg mL^{-1}) and an equimolar concentration (20 pg mL^{-1}) of each interferent were prepared in 0.01 mol L^{-1} PBS (pH 7.4). Electrochemical impedance spectroscopy (EIS) measurements were performed using the same parameters as described above. The relative response (%) was calculated for both the imaginary impedance (Z'') and absolute impedance (|Z|) at a frequency of 0.10 Hz, using the response to 5-mC alone as the reference (0%). All measurements were performed in triplicate (n=3).

Supporting Information

The Supporting Information is available free of charge at https://pubs.acs.org/doi/10.1021/

UV-Vis absorption spectra; SEM image of the poly(o-PD); Optimization of reaction/incubation times; reproducibility study; Comparison Table of Analytical Parameters.

AUTHOR INFORMATION

Corresponding author

Marcos F. S. Teixeira – *Sao Paulo State University (UNESP), School of Science and Technology, Department of Chemistry and Biochemistry, Rua Roberto Simonsen 305, 19060-900 - Presidente Prudente, SP, Brazil.*

https://orcid.org/0000-0001-9355-2143

E-mail: **marcos.fs.teixeira@unesp.br**

Authors

Pedro Costa Monteiro Pizzol – *Sao Paulo State University (UNESP), School of Science and Technology, Department of Chemistry and Biochemistry, Presidente Prudente, SP, Brazil.*

https://orcid.org/0000-0002-7037-3414

Miquéias Lima Portugal – *Sao Paulo State University (UNESP), School of Science and Technology, Department of Chemistry and Biochemistry, Presidente Prudente, SP, Brazil.*

https://orcid.org/0000-0002-3351-0459

Heitor Furlan Trevizan – *Sao Paulo State University (UNESP), School of Science and Technology, Department of Chemistry and Biochemistry, Presidente Prudente, SP, Brazil.*

https://orcid.org/0000-0002-3682-527X

Patricia Monteiro Seraphim – *Sao Paulo State University (UNESP), School of Science and Technology, Department of Physiotherapy, Presidente Prudente, SP, Brazil.*

https://orcid.org/0000-0003-2145-6640

Complete contact information is available at:
https://pubs.acs.org/10.1021/

Notes

The authors declare no competing financial interest.

ACKNOWLEDGMENT

The authors gratefully acknowledge the crucial financial support from CEPID-FAPESP (2013/07296-2) and CNPq (308232/2023-2). P.C.M.P. and M.L.P. gratefully acknowledge CAPES (88887.831630/2023-00) and FAPESP (2024/08769-6) for their master scholarships, respectively. The authors thank the Gemini language model for assistance in improving the clarity and readability of this manuscript. SJT ∴

AUTHOR CONTRIBUTIONS

Pedro Costa Monteiro Pizzol: Conceptualization, Methodology, Investigation, Visualization, Discussion, Writing - Original Draft.

Miquéias L. Portugal: Investigation, Data Discussion.

Heitor Furlan Trevizan: Data Discussion.

Patricia Monteiro Seraphim: Visualization, Discussion, Funding acquisition, Reagent suppliers.

Marcos F. S. Teixeira: Conceptualization, Methodology, Validation, Writing - Review & Editing, Supervision, Project administration, Funding acquisition.

REFERENCES

(1) Nishiyama, A.; Nakanishi, M. Navigating the DNA methylation landscape of cancer. *Trends Genet* **2021**, *37* (11), 1012-1027. DOI: 10.1016/j.tig.2021.05.002.

(2) Jin, Z. L.; Liu, Y. DNA methylation in human diseases. *Genes Dis* **2018**, *5* (1), 1-8. DOI: 10.1016/j.gendis.2018.01.002.

(3) Reddington, J. P.; Sproul, D.; Meehan, R. R. DNA methylation reprogramming in cancer: Does it act by re-configuring the binding landscape of Polycomb repressive complexes? *Bioessays* **2014**, *36* (2), 134-140. DOI: 10.1002/bies.201300130.

(4) Li, Z. J.; Tan, H.; Yu, H.; Deng, Z.; Zhou, X. B.; Wang, M. D. DNA methylation and gene expression profiles characterize epigenetic regulation of lncRNAs in colon adenocarcinoma. *J Cell Biochem* **2020**, *121* (3), 2406-2415. DOI: 10.1002/jcb.29463.

(5) Ferlay, J.; Colombet, M.; Soerjomataram, I.; Parkin, D. M.; Piñeros, M.; Znaor, A.; Bray, F. Cancer statistics for the year 2020: An overview. *Int J Cancer* **2021**, *149* (4), 778-789. DOI: 10.1002/ijc.33588.

(6) Fan, Y. X.; Liang, Y. X.; Deng, K. P.; Zhang, Z.; Zhang, G. M.; Zhang, Y. L.; Wang, F. Analysis of DNA methylation profiles during sheep skeletal muscle development using whole-genome bisulfite sequencing. *Bmc Genomics* **2020**, *21* (1), 327. DOI: 10.1186/s12864-020-6751-5.

(7) Kint, S.; De Spiegelaere, W.; De Kesel, J.; Vandekerckhove, L.; Van Criekinge, W. Evaluation of bisulfite kits for DNA methylation profiling in terms of DNA fragmentation and DNA recovery using digital PCR. *Plos One* **2018**, *13* (6), e0199091. DOI: 10.1371/journal.pone.0199091.

(8) Leitao, E.; Beygo, J.; Zeschnigk, M.; Klein-Hitpass, L.; Bargull, M.; Rahmann, S.; Horsthemke, B. Locus-Specific DNA Methylation Analysis by Targeted Deep Bisulfite Sequencing. *Methods Mol Biol* **2018**, *1767*, 351-366. DOI: 10.1007/978-1-4939-7774-1_19.

(9) Bonanni, A.; del Valle, M. Use of nanomaterials for impedimetric DNA sensors: A review. *Anal Chim Acta* **2010**, *678* (1), 7-17. DOI: 10.1016/j.aca.2010.08.022.

(10) Trevizan, H. F.; Olean-Oliveira, A.; Cardoso, C. X.; Teixeira, M. F. S. Development of a molecularly imprinted polymer for uric acid sensing based on a conductive azopolymer: Unusual approaches using electrochemical impedance/capacitance spectroscopy without

a soluble redox probe. *Sensor Actuat B-Chem* **2021**, *343*, 130141. DOI: 10.1016/j.snb.2021.130141.

(11) Olean-Oliveira, A.; Seraphim, P. M.; Teixeira, M. F. S. Methylated DNA impedimetric immunosensor based on azo-polymer-AuNPs dots and 5-methylcytosine antibody using dissolved oxygen as a redox probe. *Electrochem Commun* **2022**, *136*, 107242. DOI: 10.1016/j.elecom.2022.107242.

(12) Tekade, R. K. *Biomaterials and bionanotechnology*; Elsevier/Academic Press, 2019.

(13) Tricoli, A.; Nasiri, N.; De, S. Y. Wearable and Miniaturized Sensor Technologies for Personalized and Preventive Medicine. *Adv Funct Mater* **2017**, *27* (15), 1605271. DOI: 10.1002/adfm.201605271.

(14) Zhang, W.; Wang, R. G.; Luo, F.; Wang, P. L.; Lin, Z. Y. Miniaturized electrochemical sensors and their point-of-care applications. *Chinese Chem Lett* **2020**, *31* (3), 589-600. DOI: 10.1016/j.cclet.2019.09.022.

(15) Olean-Oliveira, A.; Brito, G. A. O.; Teixeira, M. F. S. Mechanism of Nanocomposite Formation in the Layer-by-Layer Single-Step Electropolymerization of pi-Conjugated Azopolymers and Reduced Graphene Oxide: An Electrochemical Impedance Spectroscopy Study. *Acs Omega* **2020**, *5* (40), 25954-25967. DOI: 10.1021/acsomega.0c03391.

(16) Olean-Oliveira, A.; Olean-Oliveira, T.; Moreno, A. C. R.; Seraphim, P. M.; Teixeira, M. F. S. A Chemiresistor Sensor Based on Azo-Polymer and Graphene for Real-Time Monitoring of Mitochondrial Oxygen Consumption. *Acs Sensors* **2019**, *4* (1), 118-125. DOI: 10.1021/acssensors.8b01013.

(17) Olean-Oliveira, A.; Pacheco, J. C.; Seraphim, P. M.; Teixeira, M. F. S. Synergistic effect of reduced graphene oxide/azo-polymer layers on electrochemical performance and application as nonenzymatic chemiresistor sensors for detecting superoxide anion radicals. *J Electroanal Chem* **2019**, *852*, 113520. DOI: 10.1016/j.jelechem.2019.113520.

(18) Chiba, K.; Ohsaka, T.; Ohnuki, Y.; Oyama, N. Electrochemical Preparation of a Ladder Polymer Containing Phenazine Rings. *J Electroanal Chem* **1987**, *219* (1-2), 117-124. DOI: Doi 10.1016/0022-0728(87)85034-9.

(19) Samanta, S.; Roy, P.; Kar, P. Structure and properties of conducting poly(o-phenylenediamine) synthesized in different inorganic acid medium. *Macromol Res* **2016**, *24* (4), 342-349. DOI: 10.1007/s13233-016-4054-0.

(20) Jiang, J.; Zhang, G. M.; Li, L.; Zhang, H.; Li, N.; Wang, Y. Y.; He, J.; Mao, F. J.; Yu, K. On-line monitoring of transient radicals and oligomers: o-Phenylenediamine

electrooxidation mechanism study by mass spectrometry. *Microchem J* **2020**, *153*, 104390. DOI: 10.1016/j.microc.2019.104390.
(21) Li, X. G.; Huang, M. R.; Duan, W.; Yang, Y. L. Novel multifunctional polymers from aromatic diamines by oxidative polymerizations. *Chem Rev* **2002**, *102* (9), 2925-3030. DOI: 10.1021/cr010423z.
(22) Bláha, M.; Trchová, M.; Morávková, Z.; Humpolícek, P.; Stejskal, J. Semiconducting materials from oxidative coupling of phenylenediamines under various acidic conditions. *Mater Chem Phys* **2018**, *205*, 423-435. DOI: 10.1016/j.matchemphys.2017.11.007.
(23) Wu, K. Z.; Chen, L.; Cui, W. Z.; Ruan, B.; Wu, M. X. The effect of transition metal ions (M = Mn2+, Ni2+, Co2+, Cu2+) on the chemical synthesis polyaniline as counter electrodes in dye-sensitized solar cells. *Chinese J Chem Eng* **2017**, *25* (5), 671-675. DOI: 10.1016/j.cjche.2016.10.018.
(24) Toshima, N.; Yan, H.; Ishiwatari, M. Catalytic Polymerization of Aniline and Its Derivatives by Using Copper(Ii) Salts and Oxygen - New-Type of Polyaniline with Branched Structure. *B Chem Soc Jpn* **1994**, *67* (7), 1947-1953. DOI: DOI 10.1246/bcsj.67.1947.
(25) Chan, S. K.; Lim, T. S. A straw-housed paper-based colorimetric antibody-antigen sensor. *Anal Methods-Uk* **2016**, *8* (6), 1431-1436. DOI: 10.1039/c5ay01828e.
(26) Lu, B.; Smyth, M. R.; OKennedy, R. Oriented immobilization of antibodies and its applications in immunoassays and immunosensors. *Analyst* **1996**, *121* (3), R29-R32. DOI: DOI 10.1039/an996210029r.
(27) Alves, N. A.; Olean-Oliveira, A.; Cardoso, C. X.; Teixeira, M. F. S. Photochemiresistor Sensor Development Based on a Bismuth Vanadate Type Semiconductor for Determination of Chemical Oxygen Demand. *Acs Appl Mater Inter* **2020**, *12* (16), 18723-18729. DOI: 10.1021/acsami.0c04259.
(28) Piccoli, J. P.; Santos, A.; Santos, N. A.; Lorenzón, E. N.; Cilli, E. M.; Bueno, P. R. The Self-Assembly of Redox Active Peptides: Synthesis and Electrochemical Capacitive Behavior. *Biopolymers* **2016**, *106* (3), 357-367. DOI: 10.1002/bip.22815.
(29) Bard, A. J.; Faulkner, L. R.; White, H. S. *Electrochemical methods : fundamentals and applications*, Third edition. ed.; Wiley,, 2022.
(30) Khademi, M.; Barz, D. P. J. Structure of the Electrical Double Layer Revisited: Electrode Capacitance in Aqueous Solutions. *Langmuir* **2020**, *36* (16), 4250-4260. DOI: 10.1021/acs.langmuir.0c00024.

(31) Andriianova, A. N.; Biglova, Y. N.; Mustafin, A. G. Effect of structural factors on the physicochemical properties of functionalized polyanilines. *Rsc Adv* **2020**, *10* (13), 7468-7491. DOI: 10.1039/c9ra08644g.
(32) Jarantow, S. W.; Pisors, E. D.; Chiu, M. L. Introduction to the Use of Linear and Nonlinear Regression Analysis in Quantitative Biological Assays. *Curr Protoc* **2023**, *3* (6). DOI: 10.1002/cpz1.801.
(33) Findlay, J. W. A.; Smith, W. C.; Lee, J. W.; Nordblom, G. D.; Das, I.; DeSilva, B. S.; Khan, M. N.; Bowsher, R. R. Validation of immunoassays for bioanalysis: a pharmaceutical industry perspective. *J Pharmaceut Biomed* **2000**, *21* (6), 1249-1273. DOI: Doi 10.1016/S0731-7085(99)00244-7.
(34) Mendes, C. H. S.; Silva, M. W. F.; Oliveira, S. C. B. Voltammetric determination of 5-methylcytosine at glassy carbon electrode. *J Electroanal Chem* **2021**, *895*, 115437. DOI: 10.1016/j.jelechem.2021.115437.
(35) Jiang, W. J.; Yin, H. S.; Zhou, Y. L.; Duan, J. L.; Li, H. S.; Wang, M. H.; Waterhouse, G. I. N.; Ai, S. Y. A novel electrochemiluminescence biosensor for the detection of 5-methylcytosine, TET 1 protein and β-glucosyltransferase activities based on gold nanoclusters-H2O2 system. *Sensor Actuat B-Chem* **2018**, *274*, 144-151. DOI: 10.1016/j.snb.2018.07.149.
(36) Van der Auwera, I.; Elst, H. J.; Van Laere, S. J.; Maes, H.; Huget, P.; van Dam, P.; Van Marck, E. A.; Vermeulen, P. B.; Dirix, L. Y. The presence of circulating total DNA and methylated genes is associated with circulating tumour cells in blood from breast cancer patients. *Brit J Cancer* **2009**, *100* (8), 1277-1286. DOI: 10.1038/sj.bjc.6605013.
(37) Chan, K. C. A.; Lai, P. B. S.; Mok, T. S. K.; Chan, H. L. Y.; Ding, C. M.; Yeung, S. W.; Lo, Y. M. D. Quantitative analysis of circulating methylated DNA as a biomarker for hepatocellular carcinoma. *Clin Chem* **2008**, *54* (9), 1528-1536. DOI: 10.1373/clinchem.2008.104653.
(38) Ouyang, L.; Hu, Y. W.; Zhu, L. H.; Cheng, G. J.; Irudayaraj, J. A reusable laser wrapped graphene-Ag array based SERS sensor for trace detection of genomic DNA methylation. *Biosens Bioelectron* **2017**, *92*, 755-762. DOI: 10.1016/j.bios.2016.09.072.
(39) Povedano, E.; Vargas, E.; Ruiz-Valdepeñas, V.; Torrente-Rodríguez, R. M.; Pedrero, M.; Barderas, R.; San Segundo-Acosta, P.; Peláez-García, A.; Mendiola, M.; Hardisson, D.; et al. Electrochemical affinity biosensors for fast detection of gene-specific methylations with no need for bisulfite and amplification treatments. *Sci Rep-Uk* **2018**, *8*. DOI: 10.1038/s41598-018-24902-1.

(40) Liang, Y. T.; Zhang, B.; Xue, Z. X.; Ye, X. S.; Liang, B. An electrochemical immunosensor for global DNA methylation determination using magnetic bead-based enrichment and enzymatic amplification. *Ieee Sensor* **2021**. DOI: 10.1109/Sensors47087.2021.9639719.

(41) Thonghlueng, J.; Ngernpimai, S.; Chuaephon, A.; Phanchai, W.; Wiwasuku, T.; Wanna, Y.; Wiratchawa, K.; Intharah, T.; Thanan, R.; Sakonsinsiri, C.; et al. Dual-Responsive Carbon Quantum Dots for the Simultaneous Detection of Cytosine and 5-Methylcytosine Interpreted by a Machine Learning-Assisted Smartphone. *Acs Appl Mater Inter* **2023**, *15*, 40141-40152. DOI: 10.1021/acsami.3c00785.

3.2. Material Suplementar

UV-Vis Spectroscopic Evidence for Au(III)-(*o*-PD) Complex Formation

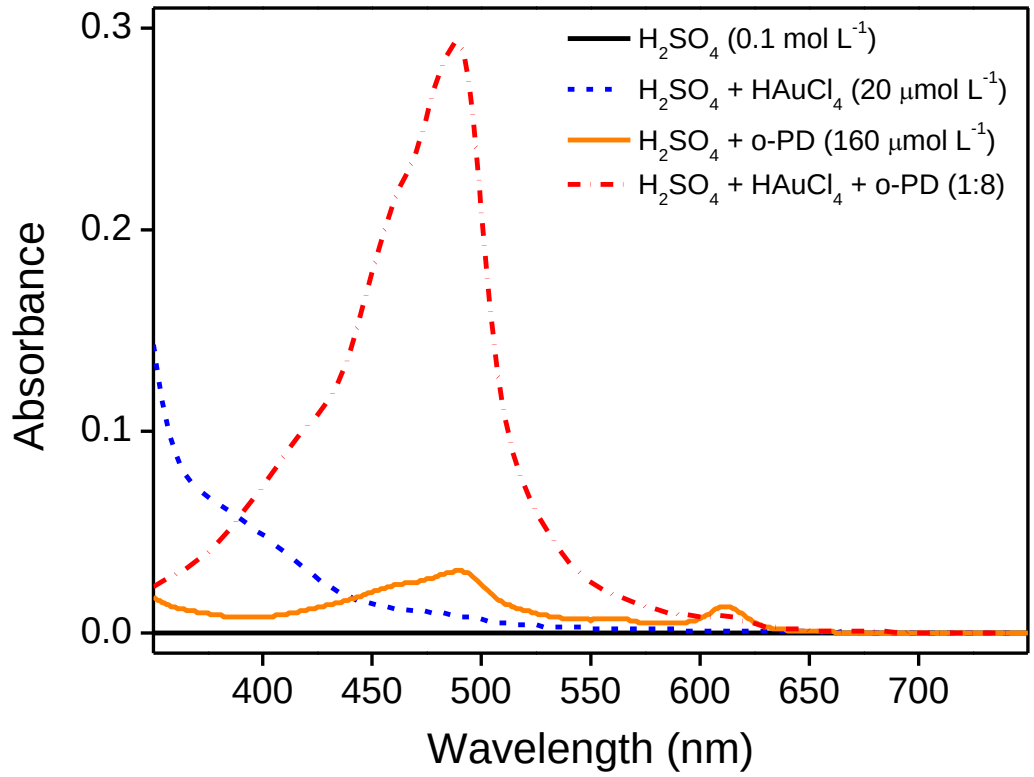

Figure S1. UV-Vis absorption spectra of: (a) 0.1 mol L^{-1} H_2SO_4 (black solid line); (b) 20 µmol L^{-1} $HAuCl_4$ in 0.1 mol L^{-1} H_2SO_4 (blue dashed line); (c) 160 µmol L^{-1} *o*-phenylenediamine (*o*-PD) in 0.1 mol L^{-1} H_2SO_4 (orange solid line); and (d) a mixture of *o*-PD (160 µmol L^{-1}) and $HAuCl_4$ (20 µmol L^{-1}) (red dashed line).

The spectrum of the mixture of o-PD and H $AuCl_4$ in 0.1 mol L^{-1} H_2SO_4 (red dashed line) exhibited significant differences compared to the spectra of the individual components. The characteristic absorption band of $[AuCl_4]^-$ at approximately 380 nm (blue

dashed line) is significantly diminished in the mixture, while a new, broad, and intense absorption band appears with a maximum around 500 nm. This new band is not present in the spectrum of o-PD alone (orange solid line). These spectral changes strongly indicate a strong interaction between Au(III) and o-PD, consistent with the formation of an Au(III)-(o-PD) complex.

Morphological Characterization of the Poly(o-phenylenediamine) Film

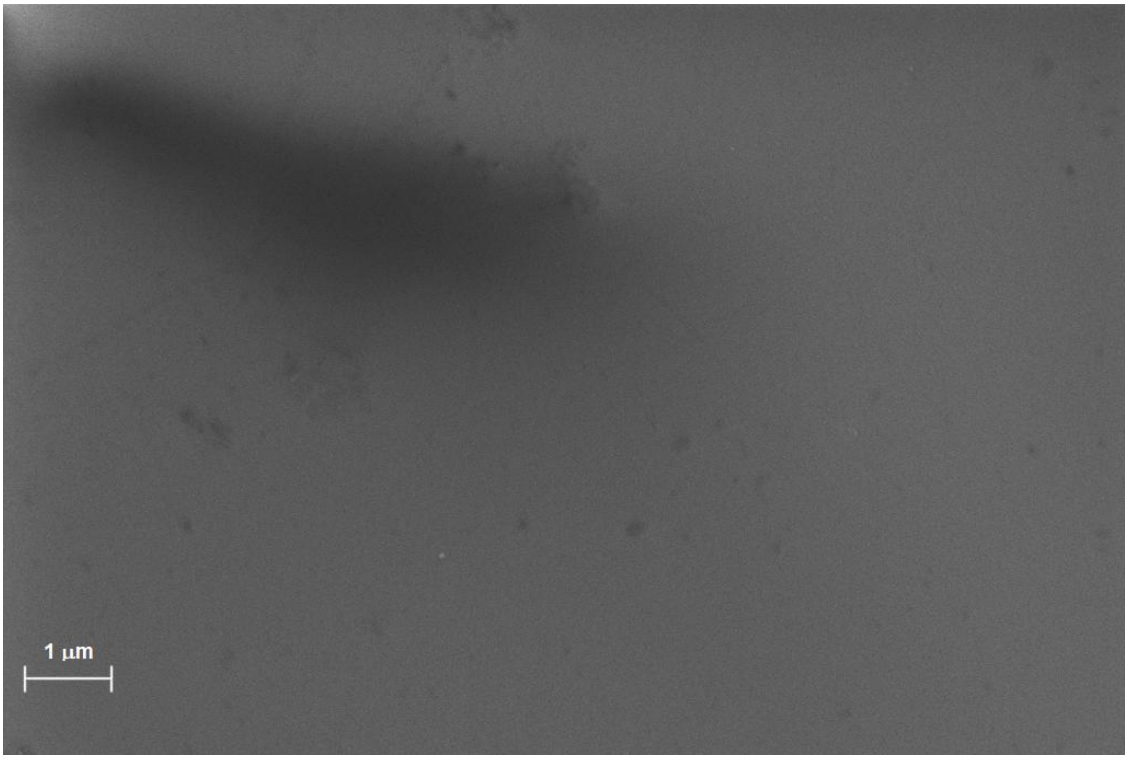

Figure S2. Scanning electron microscopy (SEM) image of the neat poly(o-phenylenediamine) electropolymerized under the same conditions as the nanocomposite film. SEM image at lower magnification (Mag: 25.00 KX, HV: 3.0 kV, scale bar = 1 µm).

The image shows a relatively smooth surface, lacking the distinct, brighter features associated with gold nanoclusters observed in the nanocomposite (Fig. 2B).

Optimization of Glutaraldehyde Reaction and Antibody Incubation Times

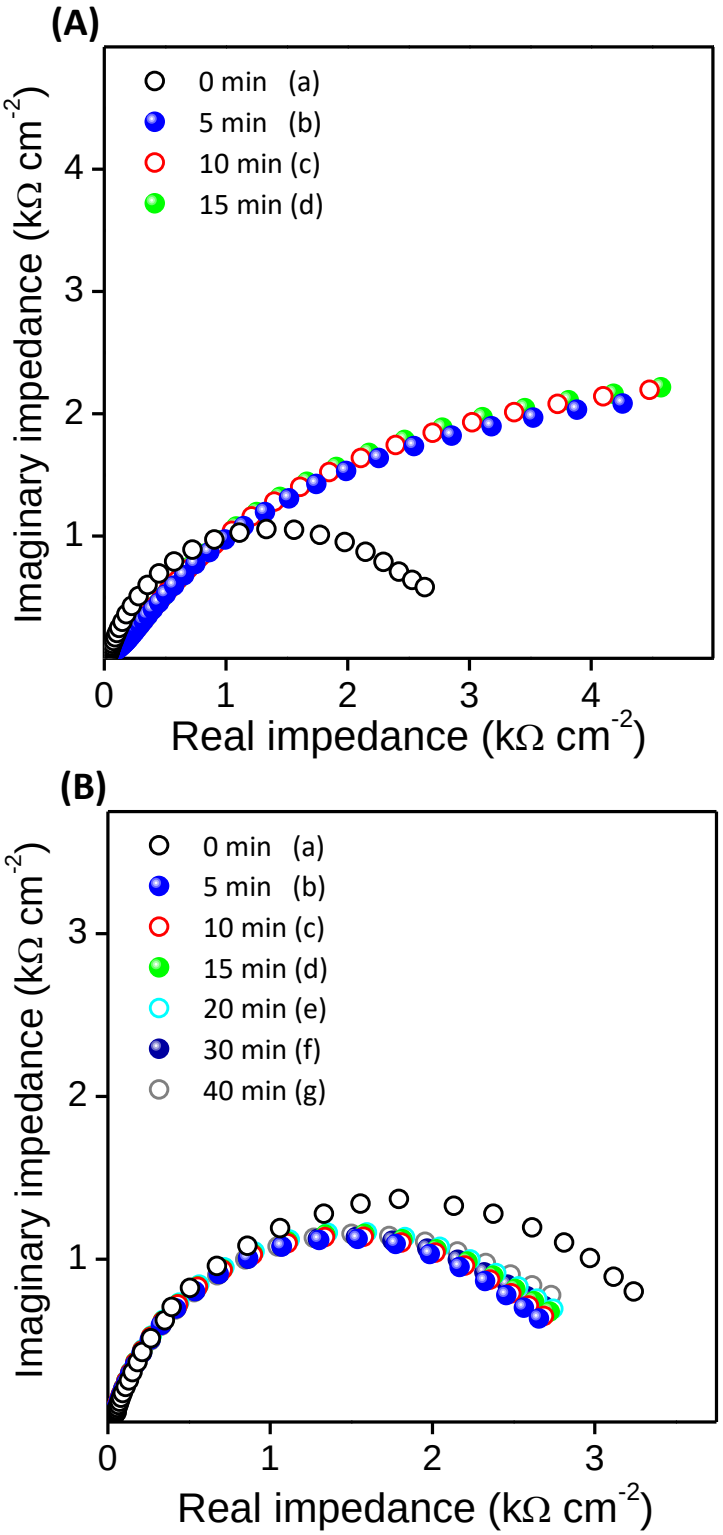

Figure S3. Optimization of reaction/incubation times. **(A)** Nyquist plots obtained for the poly(o-PD)-AuNP electrode after reaction with 1% (m/v) GA for different time intervals: (a) 0 min (black), (b) 5 mim (blue), (c) 10 min (red), (d) 15 min (green). **(B)** Nyquist plots obtained for the GA-modified electrode after incubation with 1.0 µg mL^{-1} Ab-5mC for different time intervals: (a) 0 min (black), (b) 5 mim (blue), (c) 10 min (red), (d) 15 min (green), (e) 20 min (cyan), (f) 30 mim (royal), (g) 40 min (gray). Measurements were performed in 0.01 mol L^{-1} PBS (pH 7.4) at an applied potential of -0.4 V vs. pseudo-Ag/AgCl. Frequency range: 50 kHz – 0.10 Hz.

Reproducibility of the Immunosensor Fabrication

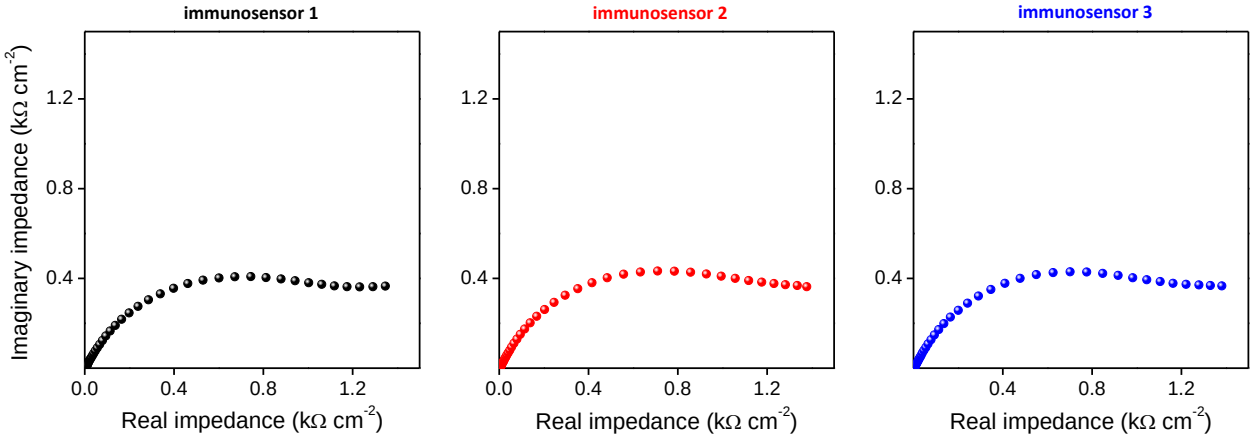

Figure S4. Assessment of the inter-electrode reproducibility of the poly(o-PD)-AuNP immunosensor. Nyquist plots obtained from three different immunosensors (labeled as Immunosensor 1, Immunosensor 2, and Immunosensor 3), fabricated independently following the same procedure. All immunosensors were exposed to a 20 pg mL^{-1} 5mC solution in 0.01 mol L^{-1} PBS (pH 7.4). The close overlap of the Nyquist plots, particularly the similar size and shape of the capacitive arcs, indicates good reproducibility in the fabrication process and consistent electrochemical response across different electrodes. Measurement conditions: Applied potential: -0.4 V vs. pseudo-Ag/AgCl; frequency range: 50 kHz – 0.10 Hz.

To assess the reproducibility of the immunosensor fabrication process, three independent poly(o-PD)-AuNP nanocomposite electrodes were prepared following the procedure described in the Experimental Section. The impedance response of each electrode to 20 pg mL^{-1} 5mC was measured using EIS under the same conditions as those used for the calibration curve. Figure S3 shows the Nyquist plots for the three independently fabricated immunosensors. The relative standard deviation (RSD) of the imaginary impedance (Z'') at 0.10 Hz was found to be 0.69%, indicating excellent reproducibility for the proposed fabrication method.

Table S1. Comparison of analytical parameters for various 5mC detection methods. The table summarizes the detection method, electrode material, linear range, limit of detection (LOD), advantages, disadvantages, and corresponding literature references. Reference numbers correspond to the numbering in the main text.

Detection Method	Sensor Material	Linear Range (pg mL^{-1})	LOD (pg mL^{-1})	Advantages	Disadvantages	Reference
Voltammetry	GCE	$0.37 \times 10^6 - 1.87 \times 10^6$	1.38×10^4	Simplicity	Low sensitivity	34
ECL	AuNPs	1.26 – 6.30	0.43	High Sensity	Small response range	35
SERS	Graphen-Ag array	$5000 - 5.0 \times 10^{-6}$	500	High sensitivity	High limit of quantification	38
Amperometry	4-ABA/AuNPs	$1.0 \times 10^6 - 2.5 \times 10^8$	7.3	Bisulfite-free	High limit of quantification	39
Amperometry	Prussian Blue-doped carbon	Not reported	Not reported	Bisulfite-free	Low sensitivity	40
Fluorescence	Carbon quantum dots	$63 \times 10^6 - 126 \times 10^6$	9.4×10^6	Detecting methylation levels in urine	High limit of quantification	41
EIS Impedance	Poly(azo-BBY)-AuNPs	5 – 120 pg mL^{-1}	0.64	No external redox probe or secondary antibodies	Low limit detection	11
EIS Impedance	Poly(o-PD)-AuNP	10 - 80	1.18	High sensitivity	Limited antibody stability	This work

Capítulo IV

Conclusão e Desafios Futuros

4.1. Conclusão

Este trabalho apresentou o desenvolvimento de uma plataforma sensorial fundamentada em um filme nanocompósito composto por poli(o-FD) e nanopartículas de ouro (AuNPs) encapsuladas. A síntese do material foi realizada por meio de eletropolimerização em etapa única, empregando dois substratos distintos com perfil voltamétrico estável e reprodutível. A espectroscopia de impedância eletroquímica foi utilizada para caracterizar os fenômenos interfaciais e comparar o desempenho eletroquímico dos filmes de poli(o-FD) e poli(o-FD)-AuNPs. A incorporação das nanopartículas de ouro promoveu um aumento significativo na sensibilidade, confirmado pelo cálculo da área ativa do eletrodo. A caracterização morfológica do nanocompósito, realizada por microscopia eletrônica de varredura (MEV), que revelou a formação de nanoclusters de ouro encapsulados pela matriz polimérica condutora.

A construção do filme nanocompósito foi bem-sucedida, e a caracterização por espectroscopia de impedância eletroquímica permitiu monitorar de forma eficiente as interações e respostas em cada etapa do processo, incluindo a imobilização de glutaraldeído, anticorpos e BSA. Essa técnica também possibilitou a construção de uma curva de calibração e o cálculo dos limites de detecção do sensor com base em múltiplos parâmetros em uma única medição, destacando a versatilidade e a robustez da metodologia.

A plataforma sensorial impedimétrica desenvolvida demonstrou desempenho excepcional, com limites de detecção bastante reduzidos, o que a torna altamente sensível para aplicações analíticas. O imunosensor foi construído em um eletrodo impresso com área de trabalho de aproximadamente 0,008 cm^2, evidenciando sua capacidade de operação em escalas miniaturizadas. Essa característica, aliada à sua alta sensibilidade e custo-benefício, reforça seu potencial para integração em dispositivos portáteis e de fácil utilização, adequados para diagnósticos rápidos e análises in situ. A metodologia adotada dispensa o uso de anticorpos secundários ou enzimas, além de exigir baixas concentrações de reagentes e amostras, o que a torna uma alternativa economicamente viável e altamente promissora para aplicações em diagnóstico, monitoramento e análise em diversas áreas. A combinação de sensibilidade, praticidade e viabilidade econômica posiciona essa plataforma como uma ferramenta analítica de grande potencial para o futuro.

Por fim, o estudo de interferentes, utilizando as bases nitrogenadas, demonstrou a alta seletividade do imunosensor, evidenciando sua capacidade de reconhecer e se ligar especificamente ao antígeno-alvo, mesmo na presença de moléculas estruturalmente semelhantes. Essa seletividade foi comprovada pela baixa variação da resposta da plataforma (abaixo de 5%) o que reforça a eficácia e a confiabilidade do anticorpo em aplicações analíticas e diagnósticas.

4.2. Desafios Futuros

Apesar dos avanços significativos alcançados com o desenvolvimento da plataforma sensorial baseada no filme nanocompósito de poli(o-FD) e nanopartículas de ouro (AuNPs), diversos desafios persistem e devem ser abordados para maximizar o potencial do método quantitativo. Um dos principais desafios é a otimização da estabilidade e da durabilidade do nanocompósito em condições operacionais variadas, especialmente em ambientes complexos, como fluidos biológicos, onde a interferência de outras moléculas pode afetar o desempenho do sensor.

Outro desafio importante é a integração da plataforma em dispositivos portáteis, que possam ser utilizados em ambientes fora do laboratório, como em pontos de atendimento ou em locais remotos. A validação clínica da plataforma em amostras reais e diversificadas é outro passo crucial para sua adoção em diagnósticos médicos. Estudos adicionais são necessários para avaliar o desempenho do sensor em diferentes matrizes biológicas, como sangue e tecidos, e para comparar sua eficácia com métodos diagnósticos já estabelecidos. Além disso, a exploração de novos biomarcadores e a adaptação da plataforma para a detecção de outras moléculas de interesse clínico podem ampliar sua aplicabilidade.

Por fim, questões relacionadas à escalabilidade da produção e ao custo-benefício do dispositivo precisam ser abordadas para garantir sua viabilidade comercial. A redução dos custos de fabricação, o uso de materiais sustentáveis e a otimização dos processos de síntese e funcionalização do nanocompósito são aspectos essenciais para a transição da tecnologia do laboratório para o mercado. Superar esses desafios permitirá que a plataforma sensorial desenvolvida se consolide como uma ferramenta analítica inovadora, contribuindo para o avanço do diagnóstico precoce, do monitoramento de doenças e da análise em diversas áreas da saúde e da pesquisa biomédica.

REFERÊNCIAS

A, B.; M, Del V. Use of nanomaterials for impedimetric DNA sensors: a review. **Analytica chimica acta**, [s. l.], v. 678, n. 1, 2010. Disponível em: https://pubmed.ncbi.nlm.nih.gov/20869498/. Acesso em: 27 abr. 2023.

BHATTACHARJEE, R.; MORIAM, S.; UMER, M.; NGUYEN, N.-T.; SHIDDIKY, M. J. A. DNA methylation detection: recent developments in bisulfite free electrochemical and optical approaches. **The Analyst**, [s. l.], v. 143, n. 20, p. 4802–4818, 2018. Disponível em: http://xlink.rsc.org/?DOI=C8AN01348A. Acesso em: 28 mar. 2023.

BHOOTRA, S.; JILL, N.; SHANMUGAM, G.; RAKSHIT, S.; SARKAR, K. **DNA methylation and cancer: transcriptional regulation, prognostic, and therapeutic perspective**, Springer, 2023.

CHEN, C.; WANG, Z.; DING, Y.; WANG, L.; WANG, S.; WANG, H.; QIN, Y. **DNA Methylation: From Cancer Biology to Clinical Perspectives**, IMR Press Limited, 2022.

CROUCH, A. M.; KHOTSENG, L. E.; POLHUIS, M.; WILLIAMS, D. R. **Comparative study of cyclic voltammetry with potentiometric analysis for determining formation constants for polyaminocarboxylate-metal ion complexesAnalytica Chimica Acta**. [s.l: s.n.].

DE LA RICA, R.; STEVENS, M. M. Plasmonic ELISA for the ultrasensitive detection of disease biomarkers with the naked eye. **Nature Nanotechnology**, [s. l.], v. 7, n. 12, p. 821–824, 2012.

DINCER, C.; BRUCH, R.; COSTA-RAMA, E.; FERNÁNDEZ-ABEDUL, M. T.; MERKOÇI, A.; MANZ, A.; URBAN, G. A.; GÜDER, F. **Disposable Sensors in Diagnostics, Food, and Environmental Monitoring**, Wiley-VCH Verlag, 2019.

E, E.; G, C.; A, E. Electrochemical assay for determination of gluten in flour samples. **Food chemistry**, [s. l.], v. 184, 2015. Disponível em: https://pubmed.ncbi.nlm.nih.gov/25872442/. Acesso em: 27 abr. 2023.

ELAHI, N.; KAMALI, M.; BAGHERSAD, M. H. **Recent biomedical applications of gold nanoparticles: A review**, Elsevier B.V., 2018.

FAN, Y.; LIANG, Y.; DENG, K.; ZHANG, Z.; ZHANG, G.; ZHANG, Y.; WANG, F. Analysis of DNA methylation profiles during sheep skeletal muscle development using whole-genome bisulfite sequencing. **BMC Genomics**, [s. l.], v. 21, n. 1, 2020.

FRISO, S.; CHOI, S. W.; DOLNIKOWSKI, G. G.; SELHUB, J. A method to assess genomic DNA methylation using high-performance liquid chromatography/electrospray ionization mass spectrometry. **Analytical Chemistry**, [s. l.], v. 74, n. 17, p. 4526–4531, 2002.

GOUIL, Q.; KENIRY, A. **Latest techniques to study DNA methylation**, Portland Press Ltd, 2019.

GUO, S.; WANG, E. **Synthesis and electrochemical applications of gold nanoparticles**, 2007.

HE, S.; YUAN, Y.; NAG, A.; FENG, S.; AFSARIMANESH, N.; HAN, T.; MUKHOPADHYAY, S. C.; ORGAN, D. R. A Review on the Use of Impedimetric Sensors for the Inspection of Food Quality. **International Journal of Environmental Research and Public Health**, [s. l.], v. 17, n. 14, p. 5220, 2020. Disponível em: https://www.mdpi.com/1660-4601/17/14/5220. Acesso em: 26 mar. 2023.

HOSSAIN, T.; MAHMUDUNNABI, G.; MASUD, M. K.; ISLAM, Md. N.; OOI, L.; KONSTANTINOV, K.; HOSSAIN, M. S. Al; MARTINAC, B.; ALICI, G.; NGUYEN, N.-T.; SHIDDIKY, M. J. A. Electrochemical biosensing strategies for DNA methylation analysis. **Biosensors and Bioelectronics**, [s. l.], v. 94, p. 63–73, 2017. Disponível em: https://linkinghub.elsevier.com/retrieve/pii/S0956566317301124. Acesso em: 26 mar. 2023.

JADOUN, S.; RIAZ, U.; YÁÑEZ, J.; PAL SINGH CHAUHAN, N. **Synthesis, characterization and potential applications of Poly(o-phenylenediamine) based copolymers and Nanocomposites: A comprehensive review**, Elsevier Ltd, 2021.

JAMKHANDE, P. G.; GHULE, N. W.; BAMER, A. H.; KALASKAR, M. G. **Metal nanoparticles synthesis: An overview on methods of preparation, advantages and disadvantages, and applications**, Editions de Sante, 2019.

JANRAO, D. M.; PATHAN, J.; KAYANDE, D. D.; MULLA, J. J. AN OVER VIEW OF POTENTIOMETRIC DETERMINATION OF STABILITY CONSTANTS OF METAL COMPLEXES. **Sci. Revs. Chem. Commun**, [s. l.], v. 4, n. 1, p. 11–24, 2014. Disponível em: www.sadgurupublications.com

JIN, Z.; LIU, Y. **DNA methylation in human diseases**, Chongqing yi ke da xue, di 2 lin chuang xue yuan Bing du xing gan yan yan jiu suo, 2018.

K, N.; ROUT, C. S. Conducting polymers: a comprehensive review on recent advances in synthesis, properties and applications. **RSC Advances**, [s. l.], v. 11, n. 10, p. 5659–5697, 2021. Disponível em: http://xlink.rsc.org/?DOI=D0RA07800J. Acesso em: 14 fev. 2023.

KHAN, I.; SAEED, K.; KHAN, I. **Nanoparticles: Properties, applications and toxicities**, Elsevier B.V., 2019.

KIZLING, M.; DZWONEK, M.; WIECKOWSKA, A.; BILEWICZ, R. **Gold nanoparticles in bioelectrocatalysis – The role of nanoparticle size**, Elsevier B.V., 2018.

KOCH, A.; JOOSTEN, S. C.; FENG, Z.; DE RUIJTER, T. C.; DRAHT, M. X.; MELOTTE, V.; SMITS, K. M.; VEECK, J.; HERMAN, J. G.; VAN NESTE, L.; VAN CRIEKINGE, W.; DE MEYER, T.; VAN ENGELAND, M. Analysis of DNA methylation in cancer: location revisited. **Nature Reviews Clinical Oncology**, [s. l.], v. 15, n. 7, p.

459–466, 2018. Disponível em: http://www.nature.com/articles/s41571-018-0004-4. Acesso em: 18 jan. 2023.

KWON, T.; GUNASEKARAN, S.; EOM, K. **Atomic force microscopy-based cancer diagnosis by detecting cancer-specific biomolecules and cells**, Elsevier B.V., 2019.

LAZANAS, A. C.; PRODROMIDIS, M. I. Electrochemical Impedance Spectroscopy─A Tutorial. **ACS Measurement Science Au**, [s. l.], 2022.

LEITÃO, E.; BEYGO, J.; ZESCHNIGK, M.; KLEIN-HITPASS, L.; BARGULL, M.; RAHMANN, S.; HORSTHEMKE, B. Locus-specific DNA methylation analysis by targeted deep bisulfite sequencing. Em: **Methods in Molecular Biology**. [s.l.] : Humana Press Inc., 2018. v. 1767p. 351–366.

LEVA-BUENO, J.; PEYMAN, S. A.; MILLNER, P. A. A review on impedimetric immunosensors for pathogen and biomarker detection. **Medical Microbiology and Immunology**, [s. l.], v. 209, n. 3, p. 343–362, 2020. Disponível em: http://link.springer.com/10.1007/s00430-020-00668-0. Acesso em: 28 fev. 2023.

LI, Y.; FAN, Z.; MENG, Y.; LIU, S.; ZHAN, H. **Blood-based DNA methylation signatures in cancer: A systematic review**, Elsevier B.V., 2023.

LIU, D.; WANG, J.; WU, L.; HUANG, Y.; ZHANG, Y.; ZHU, M.; WANG, Y.; ZHU, Z.; YANG, C. **Trends in miniaturized biosensors for point-of-care testing**, Elsevier B.V., 2020.

LOCKE, W. J.; GUANZON, D.; MA, C.; LIEW, Y. J.; DUESING, K. R.; FUNG, K. Y. C.; ROSS, J. P. DNA Methylation Cancer Biomarkers: Translation to the Clinic. **Frontiers in Genetics**, [s. l.], v. 10, p. 1150, 2019. Disponível em: https://www.frontiersin.org/article/10.3389/fgene.2019.01150/full. Acesso em: 8 fev. 2023.

LOPES, L. C.; SANTOS, A.; BUENO, P. R. An outlook on electrochemical approaches for molecular diagnostics assays and discussions on the limitations of miniaturized technologies for point-of-care devices. **Sensors and Actuators Reports**, [s. l.], v. 4, 2022.

LU, Z.; DAI, W.; LIU, B.; MO, G.; ZHANG, J.; YE, J.; YE, J. One pot synthesis of dandelion-like polyaniline coated gold nanoparticles composites for electrochemical sensing applications. **Journal of Colloid and Interface Science**, [s. l.], v. 525, p. 86–96, 2018.

MARTIN, C. S.; OLEAN-OLIVEIRA, A.; TEIXEIRA, M. F. S. A new polymeric thin film by using electropolymerization: thin film of poly(phenazine-salen) obtained from 2,2'-[1,2-ethanediylbis(nitrilomethylidyne)] -bis[4-amino-phenol]. **Journal of Electroanalytical Chemistry**, [s. l.], v. 873, 2020.

NEZAKATI, T.; SEIFALIAN, A.; TAN, A.; SEIFALIAN, A. M. **Conductive Polymers: Opportunities and Challenges in Biomedical Applications**, American Chemical Society, 2018. a.

NEZAKATI, T.; SEIFALIAN, A.; TAN, A.; SEIFALIAN, A. M. **Conductive Polymers: Opportunities and Challenges in Biomedical Applications**, American Chemical Society, 2018. b.

NISHIYAMA, A.; NAKANISHI, M. **Navigating the DNA methylation landscape of cancer**, Elsevier Ltd, 2021.

OLEAN-OLIVEIRA, A.; BRITO, G. A. O.; CARDOSO, C. X.; TEIXEIRA, M. F. S. **Nanocomposite materials based on electrochemically synthesized graphene polymers: Molecular architecture strategies for sensor applications**, MDPI AG, 2021.

OLEAN-OLIVEIRA, A.; MONTEIRO SERAPHIM, P.; TEIXEIRA, M. F. S. Methylated DNA impedimetric immunosensor based on azo-polymer-AuNPs dots and 5-methylcytosine antibody using dissolved oxygen as a redox probe. **Electrochemistry Communications**, [s. l.], v. 136, 2022.

OLEAN-OLIVEIRA, A.; OLEAN-OLIVEIRA, T.; MORENO, A. C. R.; SERAPHIM, P. M.; TEIXEIRA, M. F. S. A Chemiresistor Sensor Based on Azo-Polymer and Graphene for Real-Time Monitoring of Mitochondrial Oxygen Consumption. **ACS Sensors**, [s. l.], v. 4, n. 1, p. 118–125, 2019. a.

OLEAN-OLIVEIRA, A.; PACHECO, J. C.; SERAPHIM, P. M.; TEIXEIRA, M. F. S. Synergistic effect of reduced graphene oxide/azo-polymer layers on electrochemical performance and application as nonenzymatic chemiresistor sensors for detecting superoxide anion radicals. **Journal of Electroanalytical Chemistry**, [s. l.], v. 852, p. 113520, 2019. b. Disponível em: https://linkinghub.elsevier.com/retrieve/pii/S157266571930788X. Acesso em: 27 abr. 2023.

OLEAN-OLIVEIRA, A.; SERAPHIM, P. M.; PORTUGAL, M. L.; TEIXEIRA, M. F. S. A novel GLUT-4 electrochemical immunosensor based on a poly(thionine)-gold nanoparticle nanocomposite: Combining complex capacitance and dissolved oxygen to obtain an analytical signal. **Biosensors and Bioelectronics**, [s. l.], v. 275, 2025.

OLEAN-OLIVEIRA, A.; TEIXEIRA, M. F. S. Development of a nanocomposite chemiresistor sensor based on Π-conjugated azo polymer and graphene blend for detection of dissolved oxygen. **Sensors and Actuators, B: Chemical**, [s. l.], v. 271, p. 353–357, 2018.

PAJARES, M. J.; PALANCA-BALLESTER, C.; URTASUN, R.; ALEMANY-COSME, E.; LAHOZ, A.; SANDOVAL, J. **Methods for analysis of specific DNA methylation status**, Academic Press Inc., 2021.

PAWEŁ, K.; MAŁGORZATA, S. M. **CpG Island Methylator Phenotype—A Hope for the Future or a Road to Nowhere?**, MDPI, 2022.

PEJCIC, B.; MARCO, R. De; PARKINSON, G. The role of biosensors in the detection of emerging infectious diseases. **The Analyst**, [s. l.], v. 131, n. 10, p. 1079, 2006. Disponível em: http://xlink.rsc.org/?DOI=b603402k. Acesso em: 27 abr. 2023.

SHARMA, N. K.; NAIN, A.; SINGH, K.; RANI, N.; SINGAL, A. Impedimetric sensors: Principles, applications and recent trends. **International Journal of Innovative Technology and Exploring Engineering**, [s. l.], v. 8, n. 10, p. 4015–4025, 2019.

SHNOUDEH, A. J.; HAMAD, I.; ABDO, R. W.; QADUMII, L.; JABER, A. Y.; SURCHI, H. S.; ALKELANY, S. Z. Synthesis, Characterization, and Applications of Metal Nanoparticles. Em: **Biomaterials and Bionanotechnology**. [s.l.] : Elsevier, 2019. p. 527–612.

SKVORTSOVA, K.; STIRZAKER, C.; TABERLAY, P. **The DNA methylation landscape in cancer**, Portland Press Ltd, 2019.

SOLEYMANI, L.; LI, F. **Mechanistic Challenges and Advantages of Biosensor Miniaturization into the Nanoscale**, American Chemical Society, 2017.

TAJIK, S.; BEITOLLAHI, H.; NEJAD, F. G.; SHOAIE, I. S.; KHALILZADEH, M. A.; ASL, M. S.; VAN LE, Q.; ZHANG, K.; JANG, H. W.; SHOKOUHIMEHR, M. Recent developments in conducting polymers: applications for electrochemistry. **RSC Advances**, [s. l.], v. 10, n. 62, p. 37834–37856, 2020. Disponível em: http://xlink.rsc.org/?DOI=D0RA06160C. Acesso em: 15 fev. 2023.

TREVIZAN, H. F.; OLEAN-OLIVEIRA, A.; CARDOSO, C. X.; TEIXEIRA, M. F. S. Development of a molecularly imprinted polymer for uric acid sensing based on a conductive azopolymer: Unusual approaches using electrochemical impedance/capacitance spectroscopy without a soluble redox probe. **Sensors and Actuators, B: Chemical**, [s. l.], v. 343, 2021.

UMOREN, S. A.; SOLOMON, M. M. **Protective polymeric films for industrial substrates: A critical review on past and recent applications with conducting polymers and polymer composites/nanocomposites**, Elsevier Ltd, 2019.

XIAO, T.; HUANG, J.; WANG, D.; MENG, T.; YANG, X. **Au and Au-Based nanomaterials: Synthesis and recent progress in electrochemical sensor applications**, Elsevier B.V., 2020.

YUK, H.; LU, B.; LIN, S.; QU, K.; XU, J.; LUO, J.; ZHAO, X. 3D printing of conducting polymers. **Nature Communications**, [s. l.], v. 11, n. 1, 2020.

ZHANG, X.; LI, G.; WANG, J.; CHU, J.; WANG, F.; HU, Z.; SONG, Z. Revisiting the Structure and Electrochemical Performance of Poly(o-phenylenediamine) as an Organic Cathode Material. **ACS Applied Materials and Interfaces**, [s. l.], v. 14, n. 24, p. 27968–27978, 2022.